Article

Diverse viral cas genes antagonize CRISPR immunity

https://doi.org/10.1038/s41586-024-07923-x

Received: 11 July 2023

Accepted: 7 August 2024

Published online: 4 September 2024

Check for updates

Mark A. Katz[1,3], Edith M. Sawyer[1,3], Luke Oriolt[1], Albina Kozlova[1], Madison C. Williams[1], Shally R. Margolis[1], Matthew Johnson[2], Joseph Bondy-Denomy[2] & Alexander J. Meeske[1]✉

Prokaryotic CRISPR–Cas immunity is subverted by anti-CRISPRs (Acrs), which inhibit Cas protein activities when expressed during the phage lytic cycle or from resident prophages or plasmids[1]. Acrs often bind to specific cognate Cas proteins, and hence inhibition is typically limited to a single CRISPR–Cas subtype[2]. Furthermore, although acr genes are frequently organized together in phage-associated gene clusters[3], how such inhibitors initially evolve has remained unclear. Here we investigated the Acr content and inhibition specificity of diverse *Listeria* isolates, which naturally harbour four CRISPR–Cas systems (types I-B, II-A, II-C and VI-A). We observed widespread antagonism of CRISPR, which we traced to 11 previously unknown and 4 known acr gene families encoded by endogenous mobile elements. Among these were two Acrs that possess sequence homology to type I-B Cas proteins, one of which assembles into a defective interference complex. Surprisingly, an additional type I-B Cas homologue did not affect type I immunity, but instead inhibited the RNA-targeting type VI CRISPR system by means of CRISPR RNA (crRNA) degradation. By probing viral sequence databases, we detected abundant orphan cas genes located within putative anti-defence gene clusters. Among them, we verified the activity of a particularly broad-spectrum *cas3* homologue that inhibits type I-B, II-A and VI-A CRISPR immunity. Our observations provide direct evidence of Acr evolution by cas gene co-option, and new genes with potential for broad-spectrum control of genome editing technologies.

In response to the strong selective pressure imposed by CRISPR immunity, phages and other mobile genetic elements have evolved anti-CRISPR proteins (Acrs), which antagonize the immune effector activities of Cas proteins, removing the barrier to infection[1]. How acr genes arise within phage genomes is not well understood. Although some Acrs have enzymatic activity, and are likely to have evolved from enzymes sharing the same fold, a lack of detectable protein homology for most Acrs limits our ability to understand their origins[4–7]. One Acr (AcrIF3) has been shown to mimic the structure of the Cas protein Cas8f to block recruitment of the type I-F CRISPR nuclease Cas2-3 (refs. 8,9). AcrIF3 does not bear significant sequence homology to Cas8f; therefore, it is unknown whether this is a case of convergent evolution or whether the two proteins share a common ancestor but have diverged to the point of unrecognizable similarity. Many archaeal viruses encode homologues of Cas4, which normally plays a role in processing newly acquired spacers[10–12]. Some experimental evidence suggests that viral Cas4 proteins inhibit spacer acquisition, suggesting that cas genes might be co-opted by viruses for CRISPR antagonism[13]. Although viral CRISPR–Cas systems are diverse and abundant[14], no viral cas gene has been shown to inhibit the interference stage of immunity, and the extent of acr gene evolution from cas genes has not been explored.

Host genomes influence CRISPR function

We previously established *Listeria seeligeri* as a tractable model for studying type VI-A CRISPR–Cas immunity, and we found that *L. seeligeri* strains are also richly populated with type I-B, II-A and II-C CRISPR systems, along with many prophages and plasmids[15–18]. We sought to determine the extent to which resident mobile genetic elements and prophages affect the function of all four *Listeria* CRISPR–Cas types. We cloned each type into the site-specific integrating vector pPL2e (ref. 19) under the control of a constitutive promoter and equipped each with a spacer recognizing a target plasmid (Fig. 1a). We first introduced each of these constructs into *L. seeligeri* strain LS1 and confirmed that all four were capable of mediating sequence-specific interference against a target plasmid that was introduced by conjugation (Fig. 1b). Next, we integrated each plasmid-targeting CRISPR–Cas construct into 54 out of the 62 *L. seeligeri* strains in our laboratory's collection, then challenged each of the 216 resultant strains with a cognate target plasmid (Fig. 1c,d and Extended Data Figs. 1–4). Although each CRISPR type remained functional in some of the recipient strains, we observed frequent loss of CRISPR function among the different genetic backgrounds. The loss of CRISPR function that we observed for each type did not correlate

[1]Department of Microbiology, University of Washington, Seattle, WA, USA. [2]Department of Microbiology and Immunology, University of California San Francisco, San Francisco, CA, USA. [3]These authors contributed equally: Mark A. Katz, Edith M. Sawyer. ✉e-mail: meeske@uw.edu

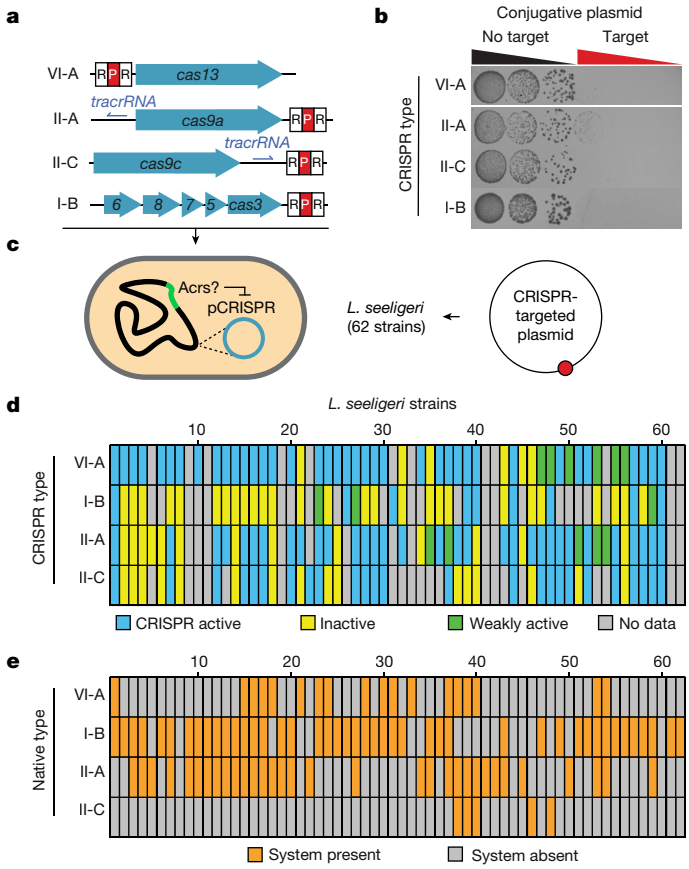

Fig. 1 | Variation in *L. seeligeri* genomes affects CRISPR–Cas function. **a**, Schematic of mobilizable chromosomally integrating CRISPR–Cas loci, each equipped with a single plasmid-targeting spacer. **b**, Plasmid-targeting assay demonstrating sequence-specific interference by all four CRISPR–Cas types in strain LS1. **c**, Schematic of strategy to detect activity of endogenous Acrs by introducing CRISPR–Cas loci into diverse strain backgrounds and challenging them with target plasmid. **d**, Functionality of four transplanted CRISPR types across 62 *L. seeligeri* strains. **e**, Natural occurrence of CRISPR types across the strain collection.

with the natural occurrence of that type in the tested strains (Fig. 1e). We observed either a partial or complete loss of CRISPR–Cas system function in 29% of strains assessed for type VI-A activity, 77% of those tested for type I-B activity (the most abundant CRISPR type in *L. seeligeri*), 36% of those tested for type II-A activity and 39% of those tested for type II-C activity (the rarest CRISPR type in our strain collection). In 27% of cases, we were unable to determine whether a particular CRISPR type was inhibited because of low conjugation efficiency of both the target plasmid and a non-targeted control (Fig. 1b, grey bars). Collectively, our findings indicate that variation in genetic background affects the function of all four CRISPR types found in *Listeria* spp.

Identification of previously unknown Acrs

Although the results above could be explained by the variable presence of unknown host factors required for CRISPR–Cas function, we hypothesized that the four CRISPR types might also be inhibited by anti-CRISPR proteins endogenously expressed by the strains in our collection. To identify such inhibitors, we took an iterative guilt-by-association bioinformatic approach that was guided by the results of our functional screen. Six type II-A inhibitor proteins and one type VI-A inhibitor have been previously identified in *Listeria* phage genomes[3,17,20], and acr genes are frequently clustered in operons associated with prophages or other mobile genetic elements[21]. Therefore, we tested genes located within predicted acr clusters for the ability to inhibit CRISPR types that could no longer mediate interference when transplanted into the cluster's host genome. First, we searched each of the *L. seeligeri* genomes in our collection for genes homologous to 81 known acr genes, which resulted in the identification of 25 predicted acr loci. (Supplementary Table 2). We examined the genes predicted to be in the same operon as known acr genes in these loci, generating a list of 33 putative anti-defence candidate gene families. Using these new candidates as queries, we searched the genomes again to find new putative anti-defence loci and anti-defence candidate genes, giving priority to genes located between previously identified candidates. We also identified predicted loci and candidate genes by searching *Listeria* genomes in publicly available databases. By exhaustively iterating this process, we expanded our dataset to 55 predicted anti-defence loci and 76 anti-defence candidate gene families residing within the 62 *L. seeligeri* genomes in our collection (Extended Data Fig. 5 and Supplementary Table 2).

Next, we investigated whether the acr gene content of each host strain correlated with loss of function for each transplanted CRISPR type (Extended Data Figs. 5–9). No known type I-B inhibitors exist in *Listeria*. However, of the 13 strains that did not support type II-A CRISPR function, all encoded at least one previously identified type II-A Acr (Extended Data Fig. 7). Conversely, only two of the 32 strains supporting type II-A function contained a cognate acr gene. Furthermore, AcrIIA1 inhibits both type II-A and type II-C immunity[22], and was present in ten of the 15 strains lacking type II-C function (Extended Data Fig. 8). Finally, the only known type VI-A acr gene (*acrVIA1*) in *Listeria* was present in a genome incompatible with type VI-A interference, and was absent from all other genomes (Extended Data Fig. 9). These data suggest that the loss of CRISPR function observed in our screen can be explained by a large set of previously unknown host-encoded Acrs. We identified anti-defence candidate genes specifically present in strains that inhibited types I-B, II-C and VI-A, and we expressed each from a plasmid in strain LS1, which does not harbour any anti-CRISPR genes. We then tested whether each candidate inhibited the matching CRISPR type in our plasmid-targeting assay (Fig. 2a). We prioritized testing of candidates that were present in inhibitory strains for a given CRISPR type but absent from strains that tolerated function of that type. We ultimately cloned 32 candidate genes, as well as seven previously identified acr genes, and tested each for inhibition of all four CRISPR types (Fig. 2b–d and Extended Data Fig. 10). Of the tested candidates that had not been previously identified, seven inhibited type I-B (hereafter, *acrIB3–9*), three inhibited type II-C (*acrIIC7–9*) and one inhibited type VI-A CRISPR immunity (*acrVIA2*) (see Supplementary Table 2 for protein sequences). Each of these Acrs was tested against each CRISPR type, but specifically inhibited only one of the four types. We also noted that an *L. seeligeri* homologue of the AcrIIA3 protein tested in our assay was a potent inhibitor of type II-C CRISPR and did not inhibit type II-A, despite being 94.3% identical to *L. monocytogenes* AcrIIA3 (Extended Data Fig. 8b). Although more than one Acr might be active in a given genome, the previously identified and newly discovered Acrs could collectively account for 68% of the inhibition observed in our functional screen.

In total, we discovered 11 new Acr families, 10 of which each had several homologues present in a variety of *Listeria* species and phages (Fig. 2e and Supplementary Fig. 2). The occurrence of these acr genes was limited to *Listeria*, except for AcrIIC9, which was also found in other *Firmicutes*, notably, *Enterococcus*. Genes encoding homologues of AcrIB3, AcrIB4, AcrIB7, AcrIB8, AcrIIC7, AcrIIC8 and AcrVIA2 were found in mobile genetic elements within *Listeria* genomes, whereas AcrIB5, AcrIB6, AcrIB7, AcrIB9 and AcrIIC9 were found in *Listeria* phage genomes. Few of these Acr proteins contained domains of known function. However, we noted that four of them contained HTH (helix-turn-helix) domains predicted to mediate DNA binding. Indeed, in addition to its CRISPR inhibition discovered here, we previously demonstrated that the gene encoding AcrIIC9 functions as a negative autoregulator of its own acr gene locus[17]. Finally, three of the Acrs

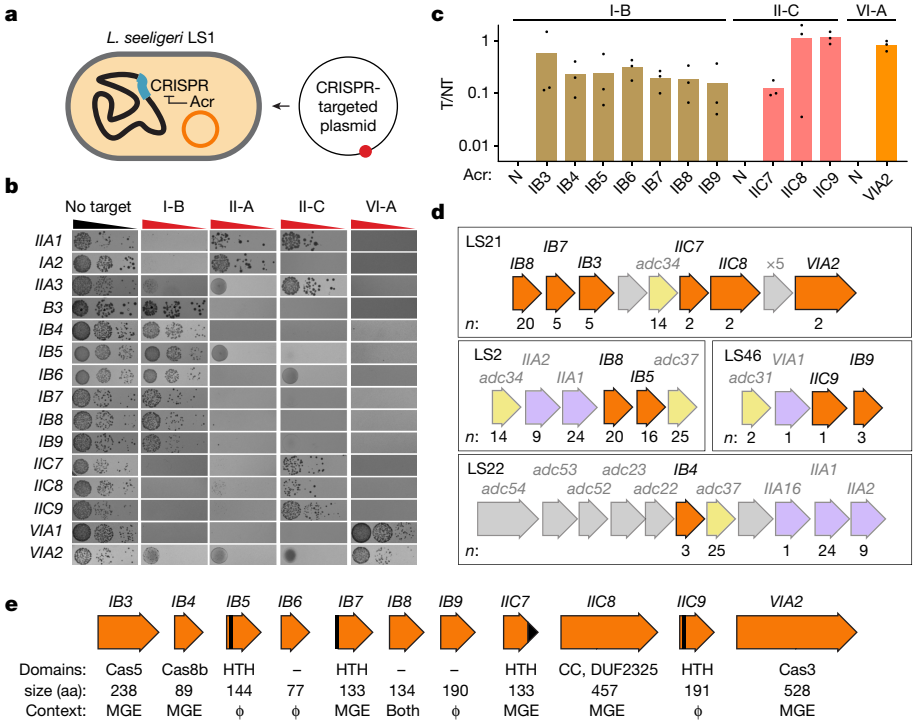

Fig. 2 | Identification of 11 type I-B, II-C and VI-A anti-CRISPR families. **a**, Schematic of strategy to test Acr candidates. Acrs were expressed from a plasmid and introduced into strain LS1 harbouring an active CRISPR–Cas system, then challenged with a target plasmid. **b**, Inhibition spectrum of tested Acrs. Each Acr candidate was tested against all four CRISPR–Cas systems in a plasmid-targeting assay. **c**, Quantification of Acr activity from three biological replicates of plasmid-targeting assay. T/NT, ratio of transconjugants with target plasmid to those with non-target plasmid. **d**, Genetic loci encoding known and previously unknown Acrs. Known Acrs are shown in purple. Anti-defence candidate genes used in prediction of acr loci are shown in yellow. Previously unknown Acrs with activity demonstrated are shown in orange. *n* represents the number of instances of the indicated gene in the *L. seeligeri* collection. **e**, Acrs discovered in this study. Predicted protein domains noted, with HTH domains depicted in black. MGE, mobile genetic element; φ, phage; aa, amino acids.

shared sequence homology with type I-B Cas proteins, which we discuss in detail below.

Cascade subunit homologue Acrs

Type I-B Cas proteins assemble into a multiprotein complex called Cascade, which contains $Cas6_1$–$Cas5_1$–$Cas8b_1$–$Cas7_7$ subunit stoichiometry[23]. Two of the newly discovered type I-B Acr proteins (AcrIB3 and AcrIB4) shared sequence homology with two type I-B Cascade subunits (Cas5 and Cas8b, respectively) (Fig. 3a). The AcrIB3 protein shares 38% identity with the full-length Cas5 protein (Supplementary Fig. 3a), whereas the AcrIB4 protein shares 38% identity with the last 90 residues of the 562-amino acid Cas8b protein (Supplementary Fig. 3b). We hypothesized that AcrIB3 and AcrIB4 might inhibit type I-B CRISPR immunity by acting as faulty subunits integrated within the Cascade complex. An alternative possibility is that expression of any individual natural Cas protein from a multicopy plasmid would interfere with Cascade complex assembly by disrupting subunit stoichiometry. To test whether this was the case, we separately expressed AcrIB3, AcrIB4 and their cognate Cas protein homologues Cas5 and Cas8b, or the C-terminal 90 amino acids of Cas8b, and tested their effect on plasmid targeting by the type I-B CRISPR system (Fig. 3b). Although the two Acrs potently inhibited interference against the target plasmid, neither bona fide Cas protein nor the Cas8b fragment affected immunity. Next, we searched for homologues of AcrIB3 and AcrIB4. In addition to numerous true Cas5 and Cas8b protein homologues, we uncovered 45 and 49 unique homologues, respectively, that were not located within CRISPR–Cas loci and were all limited to *Listeria* spp. (Fig. 3c and Supplementary Fig. 2). Our phylogenetic analysis of the proteins uncovered by this search indicated that both Acrs form their own high-confidence clades, which suggests an ancient divergence from their cognate Cas proteins. We therefore conclude that AcrIB3 and AcrIB4 are Cas protein homologues that function as inhibitors of the type I-B CRISPR–Cas system.

To investigate the mechanism by which AcrIB3 and AcrIB4 inhibit type I-B CRISPR immunity, we first tested whether they affected target DNA engagement by the Cascade complex (Fig. 3d). We designed a CRISPRi-like assay in which we deleted the nuclease *cas3* from the CRISPR locus, and then targeted Cascade to a plasmid-borne *lacZ* reporter gene in *L. seeligeri* LS1. Inactivation of *cas3* ensures that target DNA bound by Cascade is not cleaved but is transcriptionally silenced[24,25]. When we probed for *lacZ* activity by growth on plates containing X-gal, we observed CRISPR-dependent transcriptional silencing of the targeted *lacZ* gene. When we co-expressed either AcrIB3 or AcrIB4 along with Cascade, *lacZ* transcription was restored, which suggests that both anti-CRISPRs act upstream of target DNA binding by the Cascade complex and that neither functions at the level of Cas3 recruitment (Fig. 3d and Extended Data Fig. 11a).

Next, we investigated whether AcrIB3 and/or AcrIB4 affect assembly of the Cascade complex. We began by constructing a type I-B CRISPR locus containing a *cas6* allele fused to a 3×Flag tag on the C terminus. We confirmed that this fusion remained functional in interference against a plasmid with a type I-B protospacer (Extended Data Fig. 11b). We then used this construct to perform anti-Flag immunoprecipitation of the Cascade complex, in the presence and absence of AcrIB3 and AcrIB4. In the absence of Acrs, the silver-stained Cas6–3×Flag immunoprecipitate fraction contained bands consistent with the molecular weights of Cas8b, Cas7, Cas6 and Cas5, none of which was present in an untagged control sample (Fig. 3e). When we co-expressed AcrIB3 or AcrIB4, each band remained present in the immunoprecipitate, suggesting that neither Acr impedes assembly of the type I-B Cascade complex. As AcrIB3 and Cas5 have similar molecular weights, we identified the

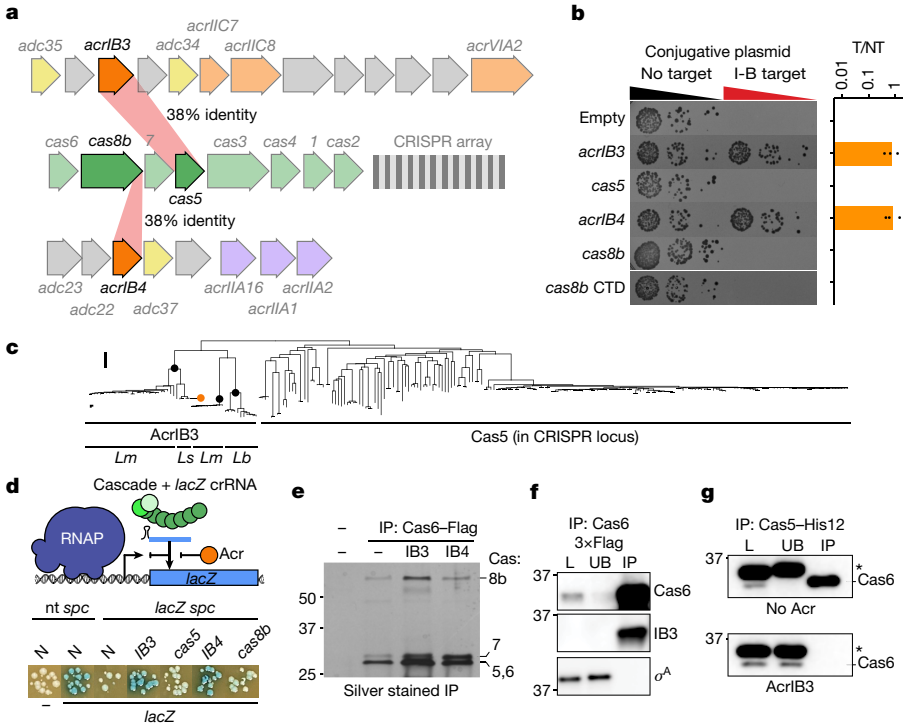

Fig. 3 | AcrIB3 and AcrIB4 are Cas protein homologues that inhibit type I-B CRISPR immunity. a, Schematic of genetic loci encoding AcrIB3 and AcrIB4 (opaque orange) and type I-B CRISPR–Cas locus. Percentage sequence identity between AcrIB3 and Cas5, and AcrIB4 and the CTD of Cas8b, is noted. **b**, Plasmid-targeting assay demonstrating that expression of AcrIB3 and AcrIB4, but not their cognate Cas proteins Cas5 and Cas8b, inhibits type I-B CRISPR immunity, and quantitation from three biological replicates. **c**, Predicted phylogeny of AcrIB3 homologues. Black circles indicate nodes with greater than 80% bootstrap support. The orange circle indicates Acr characterized experimentally. The scale bar indicates branch length (arbitrary units (a.u.)). **d**, CRISPRi *lacZ* silencing assay using a nuclease-deficient CRISPR system, demonstrating that both AcrIB3 and AcrIB4 inhibit target DNA recognition by Cascade. **e**, Silver stain analysis of Cas6–3×Flag (or untagged) immunoprecipitate fractions in the presence or absence of Acrs. Molecular weight marker, kDa. **f**, Co-immunoprecipitation of His6–AcrIB3 and Cas6–3×Flag. The housekeeping sigma factor σ^A is shown as a non-interacting control. **g**, Co-immunoprecipitation of Cas6–3×Flag with Cas5–His12 is abolished in the presence of AcrIB3. *Nonspecific Flag-reactive band. L, load; UB, unbound; IP, immunoprecipitate; nt, not-targeting. Scale bar, 0.10 a.u.

immunoprecipitated proteins by mass spectrometry (Supplementary Table 3). All Cascade subunits (Cas5, 6, 7 and 8b) were detectable regardless of Acr expression. However, in the presence of AcrIB3, we observed a decrease in the ratio of peptides mapping to Cas5 relative to those of other subunits, along with the concomitant appearance of the AcrIB3 protein (Supplementary Table 3). To further investigate whether AcrIB3 was integrated into the complex, we fused an N-terminal His6 tag onto AcrIB3, confirmed that it was functional in inhibition of plasmid targeting by type I-B CRISPR and performed immunoprecipitation of the Cascade complex in the presence of His6–AcrIB3 (Fig. 3f and Extended Data Fig. 11c). We then analysed the contents of the load, unbound and immunoprecipitated fractions by immunoblotting for Cas6–3×Flag, His6–AcrIB3 and the housekeeping sigma factor σ^A. We found that His6–AcrIB3 (but not σ^A) strongly co-immunoprecipitated with Cas6–3×Flag, which supports the conclusion that AcrIB3 assembles into the Cascade complex. Although we attempted to perform the same experiment with AcrIB4, we could not obtain a functional tagged allele. Finally, we directly tested whether AcrIB3 affects association of Cas5 with the Cascade complex. We first generated a functional type I-B CRISPR system with Cas6–3×Flag and Cas5–His12 (Extended Data Fig. 11b) and confirmed that Cas6 co-immunoprecipitated with Cas5–His12 in a nickel affinity pulldown (Fig. 3g). By contrast, we observed no Cas6 co-immunoprecipitation with Cas5 during AcrIB3 expression. Collectively, our results strongly suggest that AcrIB3 assembles into Cascade complexes in place of Cas5.

We further explored the mechanism of AcrIB3-mediated Cascade inhibition by comparing the predicted structures of AcrIB3 and Cas5. AlphaFold2-generated predictions of the Cas5 and AcrIB3 structures adopted folds similar to those of the Cas5 subunit of the experimentally determined structure of type I-A Cascade from *Pyrococcus furiosus*[26] (Extended Data Fig. 11d,e). The most pronounced predicted structural differences between AcrIB3 and Cas5 are the presence of an 18 amino acid 'hook' region in Cas5 that normally contacts Cas8 and is missing from AcrIB3 and a six amino acid extended loop specific to AcrIB3 that is predicted to contact Cas7 (Extended Data Fig. 11e–i). We generated AcrIB3 mutants in which the Cas5 hook was restored, the AcrIB3 loop was removed, or both. We observed that restoration of the hook resulted in a partial loss of Cascade inhibition, and a mutant with both of these substitutions displayed no inhibition (Extended Data Fig. 11j). Thus, we concluded that distinct structural features in AcrIB3 are necessary for its anti-CRISPR activity, and may alter interactions or structural transitions among Cascade subunits.

Cas3 homologue inhibits type VI-A CRISPR

In addition to AcrIB3 and AcrIB4, we discovered a third Acr protein (AcrVIA2) with homology to type I-B Cas proteins (Fig. 4a). AcrVIA2 shares 24% sequence identity with the helicase-nuclease Cas3 (Supplementary Fig. 4). The homology between the two proteins is centred on a shared DEAD-box helicase domain, and AcrVIA2 lacks the HD nuclease domain of Cas3. Our homology searches uncovered several true Cas3 proteins as well as eight predicted AcrVIA2 homologues not located near a CRISPR array or cas gene operon, two of which were present on *Listeria* mobile genetic elements, whereas the rest were encoded in *Myoviridae* phage genomes (Fig. 4b). Again, the Acrs formed a high-confidence phylogenetic group separate from true Cas3 proteins. Unexpectedly, we

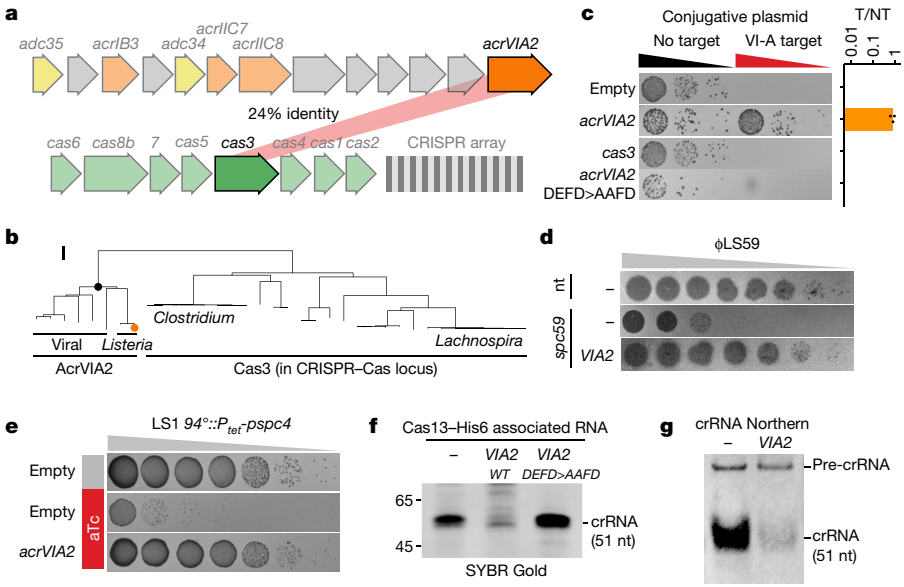

Fig. 4 | AcrVIA2 is a Cas3 homologue that inhibits type VI-A CRISPR immunity. a, Schematic of genetic loci encoding AcrVIA2 (opaque orange) and type I-B CRISPR–Cas locus. Percentage sequence identity between AcrVIA2 and Cas3 is noted. **b**, Predicted phylogeny of AcrVIA2 homologues. The black circle indicates a node with 100% bootstrap support. The orange circle indicates experimentally characterized Acr. The scale bar indicates branch length (a.u.). **c**, Plasmid-targeting assay demonstrating that expression of AcrVIA2, but not Cas3 or an AcrVIA2 DEAD-box mutant allele, inhibits type VI-A CRISPR immunity. $n = 3$ biological replicates. **d**, Plaque assay demonstrating that AcrVIA2 inhibits type VI-A immunity against a phage target. nt represents non-targeting and spc59 represents a spacer targeting an early lytic transcript of ϕLS59. The image is representative of three biological replicates. **e**, AcrVIA2 inhibits trans-RNase activity of Cas13 in vivo. Strain LS1 harbouring an aTc-inducible type VI-A protospacer, plus AcrVIA2, was plated on medium with or without aTc, as indicated. The image is representative of three biological replicates. **f**, The effect of AcrVIA2 on crRNA associated with affinity-purified Cas13–His6. Molecular weight in nucleotides. **g**, Northern blot using crRNA probe on total RNA extracted from cells with or without AcrVIA2. Scale bar, 0.20 a.u.

found that this Acr did not inhibit type I-B immunity, but instead strongly inhibited the RNA-targeting type VI-A CRISPR system (Fig. 2c). As with the two previously mentioned Cas-homologue Acrs, we confirmed that bona fide Cas3 possessed no inhibitory activity against Cas13 in a plasmid-targeting assay (Fig. 4c). When we mutated the AcrVIA2 DEAD box (DEFD>AAFD), we found that the protein remained stable yet lost inhibitory activity, which suggests that this domain is required for the function of AcrVIA2 (Fig. 4c and Extended Data Fig. 12c). Next, we tested whether AcrVIA2 could prevent Cas13 immunity against a phage target (Fig. 4d). We infected lawns of *L. seeligeri* harbouring a spacer (*spc59*) targeting the Cas13-sensitive phage ϕLS59, while co-expressing AcrVIA2 from a plasmid. Although we observed a CRISPR-dependent reduction in ϕLS59 plaque formation in this system, expression of AcrVIA2 restored phage infection in the presence of Cas13 immunity. Finally, recognition of target RNA by Cas13 stimulates a nonspecific *trans*-RNase activity that induces cell dormancy in *L. seeligeri*[16]. We tested whether AcrVIA2 affects activation of Cas13 *trans* activity using a strain harbouring an aTc-inducible, non-essential, non-coding RNA containing a protospacer recognized by *spc4* of the type VI-A CRISPR array (Fig. 4e). This strain is viable in the absence of target induction, but when plated on medium containing aTc, exhibits a strong Cas13-dependent growth defect as a consequence of nonspecific RNase activity. By contrast, co-expression of AcrVIA2 abolished Cas13-induced dormancy, and therefore prevents cleavage of target and non-target RNA.

Next, we investigated the mechanism of Cas13 inhibition by AcrVIA2. We first attempted to detect a physical interaction between both proteins. However, we were unable to detect co-immunoprecipitation of Cas13–His6 along with a partially functional AcrVIA2–3×Flag allele (Extended Data Fig. 12a,b), which suggests that, unlike AcrVIA1, AcrVIA2 does not form a stable interaction with Cas13. Accordingly, we tested whether AcrVIA2 affects the assembly of the Cas13–crRNA ribonucleoprotein complex. We immunoprecipitated a functionally tagged Cas13–3×Flag allele in the presence and absence of AcrVIA2, and then purified RNA from the isolated protein and analysed it by SYBR Gold staining (Fig. 4f). We detected an RNA band corresponding to the mature 51 nt crRNA (confirmed by northern blot; Extended Data Fig. 12d) in the immunoprecipitated Cas13 fraction, but this band was strongly reduced in cells expressing AcrVIA2. Conversely, the AcrVIA2 DEAD-box mutant did not affect Cas13-associated crRNA levels. We then performed northern blots with crRNA-specific probes on total RNA samples extracted from cells with or without AcrVIA2 (Fig. 4g). We observed a marked AcrVIA2-dependent decrease in mature crRNA, but no effect on levels of unprocessed pre-crRNA. We observed no accumulation of pre-crRNA, which suggests that AcrVIA2 does not prevent crRNA processing, nor does it affect pre-crRNA transcription. Finally, we tested whether AcrVIA2 can remove crRNA from preformed RNP complexes. We incubated lysates expressing Cas13–His6 mixed with lysates expressing AcrVIA2, and then immunoprecipitated Cas13 and analysed RNA content (Extended Data Fig. 12e). In contrast to the in vivo analyses, AcrVIA2 had no effect on crRNA levels of pre-assembled Cas13–crRNA complexes. Collectively, these results suggest that AcrVIA2 inhibits Cas13 by type VI-A crRNA degradation, in a mechanism that depends on its DEAD-box motif.

Viral cas genes reside in anti-defence loci

Our discovery of three unique Acrs homologous to type I-B Cas proteins prompted us to perform bioinformatic searches for other viral cas genes that might play anti-defence roles. We used 536 Cas protein query sequences to probe for cas genes present in the IMGVR database of high-confidence viral genomes[27]. To enrich for putative Acrs, we then removed all hits containing nearby predicted CRISPR arrays or high-confidence cas gene operons. We further eliminated all genes located within 1 kb of DNA contig ends and genes that shared greater than 90% nucleotide sequence identity with an existing hit. Ultimately, our analysis yielded 358 predicted orphan viral cas genes, representing

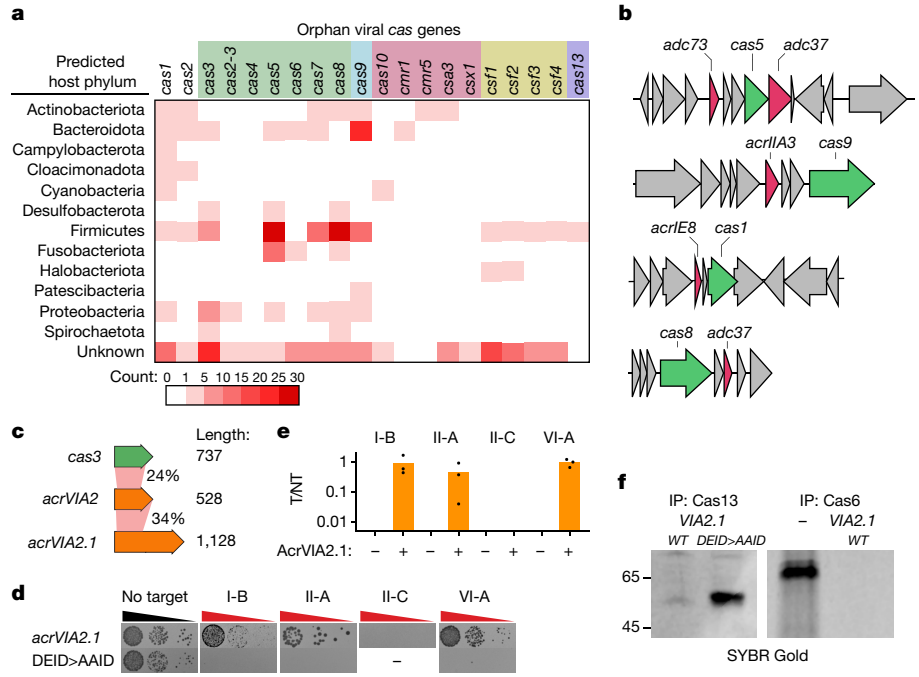

Fig. 5 | Diverse viral cas genes reside in putative anti-defence loci. **a**, Frequency of orphan viral cas genes found in the IMGVR database, organized by Cas protein query and predicted viral host phylum. Cas queries are coloured by CRISPR type (green, type I; blue, type II; pink, type III; yellow, type IV; purple, type VI). **b**, Example locus schematics for viral cas genes found in the vicinity of known anti-CRISPRs or other predicted anti-defence genes. **c**, Schematic showing percentage amino acid identity between *L. seeligeri* Cas3, the indicated Acrs and each other, along with protein lengths. **d**, Plasmid-targeting assay demonstrating the CRISPR inhibition spectrum of viral Cas3 protein and dependence on DEAD box. **e**, Quantitation of plasmid-targeting assay (three biological replicates). **f**, Effect of AcrVIA2.1 on levels of crRNA affinity-purified with Cas13–His6 or Cas6–3×Flag. Molecular weight in nucleotides.

components of types I, II, III, IV and VI CRISPR–Cas systems (Fig. 5a and Supplementary Table 4). The predicted hosts infected by viruses harbouring orphan cas genes included most bacterial phyla, with Firmicutes and Bacteroidota phages being particularly abundant. Although we cannot exclude the possibility that the viral Cas1 genes detected in our screen represent closely related casposons[28], our search was performed with sufficient stringency to avoid other Cas protein ancestors such as IscB and TnpB[29]. We found that several of the predicted viral cas genes were located next to known acr genes or predicted anti-defence candidates from our analysis in *Listeria*, which supports the idea that some of the cas homologues in our dataset play anti-CRISPR roles (Fig. 5b and Supplementary Fig. 5).

To investigate this, we selected acr gene candidates with homology to *Listeria* cas genes and tested their ability to inhibit plasmid targeting by the relevant CRISPR types (Fig. 5c,d and Extended Data Fig. 10). Among the tested candidates was a *cas3* homologue encoded on a *Myoviridae* genome. Like AcrVIA2, this protein shared limited identity (approximately 24%) with the DEAD-box helicase domain of *L. seeligeri* Cas3, shared less than 40% sequence identity with AcrVIA2 (Fig. 5c) and contained no additional domains of known function. Finally, although AcrVIA2 is similar in length to Cas3, the viral Cas3 homologue identified in our bioinformatic search was over twice the size, at 1,128 amino acids. We first tested the ability of the viral Cas3 homologue to inhibit type VI-A CRISPR immunity against a targeted plasmid, and we found that it abolished Cas13-dependent interference. Owing to its homology to AcrVIA2, we refer to it as AcrVIA2.1. Next, we tested the inhibition spectrum of AcrVIA2.1 against the four *Listeria* CRISPR–Cas types (Fig. 5d,e). Unlike AcrVIA2, AcrVIA2.1 mediated strong inhibition of types VI-A, I-B and II-A CRISPR interference. Thus, of all anti-CRISPRs characterized to date, AcrVIA2.1 has both the largest size and Cas protein inhibition spectrum. We also noted that AcrVIA2 possessed very weak inhibitory activity against types I-B and II-A, which suggests a shared capacity for broad-spectrum inhibition within this Acr family. As with AcrVIA2, analysis of Cas13-associated RNA (or Cascade-associated RNA) revealed an AcrVIA2.1-mediated decrease in crRNAs that was abolished in a DEAD-box mutant (Fig. 5f and Extended Data Fig. 12c,d). Collectively, our results suggest that there has been extensive acr gene evolution from cas genes, and that searching for orphan cas gene homologues in viral genomes is a useful approach to bioinformatically identify new anti-defence gene loci.

Discussion

In this study, we investigated the occurrence of anti-CRISPR-mediated inhibition across a large collection of bacterial isolates and four CRISPR–Cas types. Our results suggest the existence of widespread CRISPR antagonism present among *Listeria seeligeri* strains, which can be accounted for by four known and 11 previously unidentified Acr families. Three of these Acrs bear sequence identity to type I-B Cas subunits, which suggests that each Acr shares a common ancestor with its cognate Cas component. Our investigation of the mechanisms of these Acrs suggest that: (1) AcrIB3 inhibits type I-B CRISPR immunity by replacing Cas5 in a defective Cascade interference complex that fails to engage target DNA; and (2) AcrVIA2 inhibits type VI-A CRISPR immunity by causing crRNA degradation. Although AcrVIA2 may degrade crRNAs directly, our evidence does not exclude the possibility that AcrVIA2 prevents loading of crRNAs into Cas13, leading to their degradation by housekeeping nucleases. To investigate the generality of Acr evolution from Cas proteins, we probed the IMGVR database for the existence of orphan viral cas genes. We uncovered hundreds of examples of viral cas genes that were not associated with a CRISPR array or complete cas gene operon, instead residing near putative anti-defence genes. We experimentally confirmed that at least one of these genes (AcrVIA2.1) exhibits exceptionally broad-spectrum inhibition of CRISPR–Cas immunity in *L. seeligeri*. In addition to uncovering numerous anti-CRISPR proteins that could potentiate phage therapy or gene editing safety, our

findings demonstrate that diverse viruses have co-opted cas genes for CRISPR antagonism, and they provide a new strategy for the unbiased identification of counterdefence genes in prokaryotes.

Our results raise several questions regarding the evolutionary trajectories that could convert a host-encoded cas gene to a phage-encoded acr. First, how do phages capture cas genes? One possibility is by imprecise excision of temperate phages integrated near CRISPR–Cas loci. During induction of such prophages, cas genes could occasionally be packaged into viral capsids along with the phage genome. Varble and colleagues[30] recently demonstrated that some *Streptococcus* phages integrate directly into the degenerate repeats of type II-A CRISPR arrays and can sometimes capture and mobilize spacer sequences. It remains to be seen whether such a mechanism could also promote viral capture of whole cas genes or fragments thereof. Once a cas gene is integrated into a phage genome, it may not immediately play a role in CRISPR antagonism. Instead, viral cas genes might stimulate CRISPR immunity to play a protective role for lysogenized hosts that could otherwise be infected by a second phage. Next, how is a viral cas gene exapted into an anti-CRISPR? Because Cas proteins naturally make interactions with other Cas proteins, crRNA and target nucleic acids, they are well poised to evolve into inhibitors that block CRISPR immunity. Any phage-encoded Cas protein that interacts with two or more components of the CRISPR RNP might develop inhibitory activity by simply losing one of these interactions while maintaining another, resulting in a faulty Cas subunit that inactivates immunity. One benefit of this strategy (as compared with non-Cas anti-CRISPRs) is that it may be difficult for CRISPR systems to evolve resistance against such inhibitors, because they resemble the very Cas components used for immunity. In a striking parallel to our findings, Camara-Wilpert and colleagues recently described RNA anti-CRISPRs homologous to crRNAs, which act by displacement of guide RNAs from Cas nucleases[31]. Collectively, these findings and our results indicate that viral immune subversion strategies include mimicry of both RNA and protein components of the CRISPR machinery, and they also raise the possibility that subunits of anti-phage immune systems beyond CRISPR may also serve as raw material for counterdefence evolution.

In this study, we uncovered a total of 11 anti-CRISPR families present in *Listeria* prophages and mobile genetic elements. Residing beside these acr genes were 64 additional anti-defence candidate genes, 26 of which exhibited no detectable CRISPR inhibition in our assay (Supplementary Table 2). Although some of these genes may serve other functions, their frequent co-occurrence with and proximity to acr genes suggests that many could play an anti-defence role, possibly against one or more of the other antiviral defence systems found in *Listeria* spp.

Although CRISPR–Cas systems are abundant in *Listeria* spp., our functional screen revealed that most are inhibited by endogenous Acrs. Such frequent inhibition is likely to provide a selective pressure to acquire new diverse immune systems not susceptible to existing Acrs. For example, although we observed inhibition of the highly abundant type I-B CRISPR in 77% of the tested *L. seeligeri* strains, the less common type VI-A system was only inhibited in 29% of strains. If inhibition is widespread, why are CRISPR systems retained by the host? On the contrary, recent evidence suggests that prophage-encoded Acrs promote retention of host CRISPR–Cas systems, by preventing autoimmune cleavage of targets within the integrated prophage[32]. Maintenance of functional CRISPR immunity despite the presence of Acrs could provide a fitness benefit in the event that the host becomes cured of the prophage or mobile genetic element harbouring acr genes. In total, our findings represent an example of the diversity of evolved interactions in the ongoing phage–host arms race.

Online content

Any methods, additional references, Nature Portfolio reporting summaries, source data, extended data, supplementary information, acknowledgements, peer review information; details of author contributions and competing interests; and statements of data and code availability are available at https://doi.org/10.1038/s41586-024-07923-x.

1. Bondy-Denomy, J., Pawluk, A., Maxwell, K. L. & Davidson, A. R. Bacteriophage genes that inactivate the CRISPR/Cas bacterial immune system. *Nature* **493**, 429–432 (2013).
2. Bondy-Denomy, J. et al. Multiple mechanisms for CRISPR–Cas inhibition by anti-CRISPR proteins. *Nature* **526**, 136–139 (2015).
3. Rauch, B. J. et al. Inhibition of CRISPR–Cas9 with bacteriophage proteins. *Cell* **168**, 150–158 e110 (2017).
4. Knott, G. J. et al. Broad-spectrum enzymatic inhibition of CRISPR–Cas12a. *Nat. Struct. Mol. Biol.* **26**, 315–321 (2019).
5. Dong, L. et al. An anti-CRISPR protein disables type V Cas12a by acetylation. *Nat. Struct. Mol. Biol.* **26**, 308–314 (2019).
6. Niu, Y. et al. A type I-F anti-CRISPR protein inhibits the CRISPR–Cas surveillance complex by ADP-ribosylation. *Mol. Cell* **80**, 512–524 e515 (2020).
7. Sahakyan, H., Makarova, K. S. & Koonin, E. V. Search foroOrigins of anti-CRISPR proteins by structure comparison. *CRISPR J.* **6**, 222–231 (2023).
8. Chowdhury, S. et al. Structure reveals mechanisms of viral suppressors that intercept a CRISPR RNA-guided surveillance complex. *Cell* **169**, 47–57 e11 (2017).
9. Rollins, M. F. et al. Structure reveals a mechanism of CRISPR-RNA-guided nuclease recruitment and anti-CRISPR viral mimicry. *Mol. Cell* **74**, 132–142 e135 (2019).
10. Krupovic, M., Cvirkaite-Krupovic, V., Prangishvili, D. & Koonin, E. V. Evolution of an archaeal virus nucleocapsid protein from the CRISPR-associated Cas4 nuclease. *Biol. Direct* **10**, 65 (2015).
11. Hudaiberdiev, S. et al. Phylogenomics of Cas4 family nucleases. *BMC Evol. Biol.* **17**, 232 (2017).
12. Goodman, D. A. & Stedman, K. M. Comparative genetic and genomic analysis of the novel fusellovirus Sulfolobus spindle-shaped virus 10. *Virus Evol.* **4**, vey022 (2018).
13. Zhang, Z., Pan, S., Liu, T., Li, Y. & Peng, N. Cas4 nucleases can effect specific integration of CRISPR spacers. *J. Bacteriol.* **201**, e00747–18 (2019).
14. Al-Shayeb, B. et al. Diverse virus-encoded CRISPR–Cas systems include streamlined genome editors. *Cell* **185**, 4574–4586 e4516 (2022).
15. Meeske, A. J. & Marraffini, L. A. RNA guide complementarity prevents self-targeting in type VI CRISPR systems. *Mol. Cell* **71**, 791–801 e793 (2018).
16. Meeske, A. J., Nakandakari-Higa, S. & Marraffini, L. A. Cas13-induced cellular dormancy prevents the rise of CRISPR-resistant bacteriophage. *Nature* **570**, 241–245 (2019).
17. Meeske, A. J. et al. A phage-encoded anti-CRISPR enables complete evasion of type VI-A CRISPR–Cas immunity. *Science* **369**, 54–59 (2020).
18. Williams, M. C. et al. Restriction endonuclease cleavage of phage DNA enables resuscitation from Cas13-induced bacterial dormancy. *Nat. Microbiol.* **8**, 400–409 (2023).
19. Lauer, P., Chow, M. Y., Loessner, M. J., Portnoy, D. A. & Calendar, R. Construction, characterization, and use of two Listeria monocytogenes site-specific phage integration vectors. *J. Bacteriol.* **184**, 4177–4186 (2002).
20. Mahendra, C. et al. Broad-spectrum anti-CRISPR proteins facilitate horizontal gene transfer. *Nat. Microbiol.* **5**, 620–629 (2020).
21. Osuna, B. A. et al. Critical anti-CRISPR locus repression by a bi-functional Cas9 inhibitor. *Cell Host Microbe* **28**, 23–30 e25 (2020).
22. Osuna, B. A. et al. Listeria phages induce Cas9 degradation to protect lysogenic genomes. *Cell Host Microbe* **28**, 31–40 e39 (2020).
23. Lu, M. et al. Structure and genome editing of type I-B CRISPR–Cas. *Nat. Commun.* **15**, 4126 (2024).
24. Luo, M. L., Mullis, A. S., Leenay, R. T. & Beisel, C. L. Repurposing endogenous type I CRISPR–Cas systems for programmable gene repression. *Nucleic Acids Res.* **43**, 674–681 (2015).
25. Rath, D., Amlinger, L., Hoekzema, M., Devulapally, P. R. & Lundgren, M. Efficient programmable gene silencing by Cascade. *Nucleic Acids Res.* **43**, 237–246 (2015).
26. Hu, C. et al. Allosteric control of type I-A CRISPR-Cas3 complexes and establishment as effective nucleic acid detection and human genome editing tools. *Mol. Cell* **82**, 2754–2768 e2755 (2022).
27. Camargo, A. P. et al. IMG/VR v4: an expanded database of uncultivated virus genomes within a framework of extensive functional, taxonomic, and ecological metadata. *Nucleic Acids Res.* **51**, D733–D743 (2023).
28. Krupovic, M., Makarova, K. S., Forterre, P., Prangishvili, D. & Koonin, E. V. Casposons: a new superfamily of self-synthesizing DNA transposons at the origin of prokaryotic CRISPR–Cas immunity. *BMC Biol.* **12**, 36 (2014).
29. Kapitonov, V. V., Makarova, K. S. & Koonin, E. V. ISC, a novel group of bacterial and archaeal DNA transposons that encode Cas9 homologs. *J. Bacteriol.* **198**, 797–807 (2015).
30. Varble, A. et al. Prophage integration into CRISPR loci enables evasion of antiviral immunity in *Streptococcus pyogenes*. *Nat. Microbiol.* **6**, 1516–1525 (2021).
31. Camara-Wilpert, S. et al. Bacteriophages suppress CRISPR–Cas immunity using RNA-based anti-CRISPRs. *Nature* **623**, 601–607 (2023).
32. Rollie, C. et al. Targeting of temperate phages drives loss of type I CRISPR–Cas systems. *Nature* **578**, 149–153 (2020).

Methods

Bacterial strains and growth conditions

L. seeligeri strains were cultured in Brain Heart Infusion (BHI) medium at 30 °C. Where appropriate, BHI was supplemented with the following antibiotics for selection: nalidixic acid (50 μg ml^{-1}), chloramphenicol (10 μg ml^{-1}), erythromycin (1 μg ml^{-1}) or kanamycin (50 μg ml^{-1}). For cloning, plasmid preparation and conjugative plasmid transfer, *Escherichia coli* (*E. coli*) strains were cultured in Lysogeny Broth (LB) medium at 37 °C. Where appropriate, LB was supplemented with the following antibiotics: ampicillin (100 μg ml^{-1}), chloramphenicol (25 μg ml^{-1}) and kanamycin (50 μg ml^{-1}). For conjugative transfer of *E. coli*–*Listeria* shuttle vectors, plasmids were purified from Turbo Competent *E. coli* (New England Biolabs) and transformed into the *E. coli* conjugative donor strains SM10 λ*pir* or S17 λ*pir*. For a list of strains used in this study, see Supplementary Table 1.

Plasmid construction and preparation

All genetic constructs for expression in *L. seeligeri* were cloned into the following three compatible shuttle vectors, each of which contains an origin of transfer sequence for mobilization by transfer genes of the IncP-type plasmid RP4. These transfer genes are integrated into the genome of the *E. coli* conjugative donor strains SM10 λ*pir* or S17 λ*pir*. All plasmids used in this study, along with details of their construction can be found in Supplementary Table 1.

pPL2e: ectopically integrating plasmid conferring chloramphenicol resistance in *E. coli* and erythromycin resistance in *Listeria*; integrates into the tRNA^{Arg} locus in the *L. seeligeri* chromosome[19].

pAM8: *E. coli*–*Listeria* shuttle vector conferring ampicillin resistance in *E. coli* and chloramphenicol resistance in *Listeria*[15].

pAM326: *E. coli*–*Listeria* shuttle vector conferring kanamycin resistance in *E. coli* and *Listeria*[17].

Mobilizable CRISPR–Cas systems were constructed by cloning the type I-B, II-A, II-C and VI-A CRISPR–Cas loci into pPL2e, each equipped with a spacer matching a target plasmid. Target plasmids were derived from pAM8. In the case of type II-A, one variant of the CRISPR–Cas plasmid harboured a spacer targeting a protospacer region on pAM8 followed by an NGG PAM, and a separate CRISPR plasmid harboured a non-targeting spacer. The same approach was taken for type II-C, except the protospacer region was followed by an NNGCAA PAM. For types I-B and VI-A, naturally occurring spacers were used in the CRISPR plasmid, and matching protospacers were inserted into pAM8. The type I-B protospacer was preceded by a 5′ CCN protospacer adjacent motif (PAM) sequence. The type VI-A protospacer was inserted into a transcribed region in the 3′ untranslated region of the chloramphenicol resistance gene of pAM8.

Putative anti-CRISPR constructs were assembled by cloning into NcoI/EagI digested pAM551, which is derived from pAM326 and contains an aTc-inducible P_{tet} promoter.

E. coli–*L. seeligeri* conjugation

All genetic constructs for expression in *L. seeligeri* were introduced by conjugation with *E. coli* donor strains SM10 λ*pir* or S17 λ*pir*. We diluted 100 μl of each donor and recipient culture into 10 ml BHI medium and concentrated it on a 0.45 μm porosity filter disk using vacuum filtration. Filter discs were laid onto BHI agar supplemented with oxacillin (8 μg ml^{-1} for pPL2e or pAM326 derived plasmids and 128 μg ml^{-1} for pAM8 derived plasmids), which weakens the cell wall and enhances conjugation, and then incubated at 37 °C for 4 h. Cells were resuspended in 2 ml BHI and serially diluted, and transconjugants were selected on BHI medium containing 50 μg ml^{-1} nalidixic acid (which kills donor *E. coli* but not recipient *L. seeligeri)* in addition to the appropriate antibiotic for plasmid selection. Transconjugants were isolated after 2–3 days of incubation at 30 °C.

Phylogenetic tree construction

To reconstruct Acr phylogeny, query Acr proteins were searched against the BLAST nr database[33] using an *E*-value cutoff of 5×10^{-3} (for AcrIB4) or 1×10^{-4} (for all other Acrs). The top 250 hits were aligned using T-Coffee[34]. For AcrIB4, only the C-terminal 90 amino acids were included for alignment, as this is the region with shared homology between AcrIB4 and the much larger Cas8b. Phylogenetic trees and bootstrap values were calculated using MEGA (v.11)[35], using the neighbour-joining method with 1,000 bootstrap replications.

Co-immunoprecipitation

L. seeligeri harbouring Flag-tagged and/or His6-tagged proteins was cultured in 30 ml BHI to saturation, and then pelleted by centrifugation. Cells were resuspended in 1.5 ml lysis buffer containing 50 mM HEPES pH 7, 150 mM NaCl, 5 mM $MgCl_2$, 5% glycerol, 1 mM PMSF and 2 mg ml^{-1} lysozyme, and then incubated at 37 °C for 20 min. Lysis was performed by sonication, and then insoluble material was pelleted by centrifugation at 15,000 rpm for 10 min. The clarified supernatants were sampled (load fraction), then applied to 40 μl of buffer-equilibrated M2 anti-Flag antibody affinity resin (Sigma-Aldrich) and incubated at 4 °C for 2 h. Flag resin was pelleted by centrifugation at 1,000 rpm for 1 min, and the supernatant was sampled (unbound fraction). Flag resin was washed three times for 5 min each with 1 ml wash buffer (50 mM HEPES pH 7, 150 mM NaCl, 5 mM $MgCl_2$, 5% glycerol). Finally, the immunoprecipitated fraction was eluted with 40 μl of 0.1 mg ml^{-1} 3xFlag peptide (Sigma-Aldrich) at room temperature. Cas5–His12 was purified by nickel affinity pulldown, using the protocol above, except with Ni^{++}-NTA agarose beads. The wash buffer for Cas5–His12 purification contained 10 mM imidazole, and the elution buffer contained 250 mM imidazole. All samples were denatured by dilution in 2× Laemmli sample buffer containing 4% SDS and 10% beta-mercaptoethanol. Load, unbound and IP fractions were analysed by immunoblot using anti-Flag (Sigma-Aldrich), anti-His6 (Genscript) and anti-σ^A (gift of David Rudner, Harvard Medical School) antibodies. Silver staining was performed on 12 μl of each immunoprecipitate sample, using the Pierce Silver Staining Kit (Thermo Fisher) according to the manufacturer's instructions.

Analysis of Cas13-associated crRNA

L. seeligeri cultures harbouring *cas13-his6* and/or *acrVIA2* were grown to saturation. A 50 ml culture was harvested, pelleted at 4,300 rpm and frozen at −80 °C. Pellets were resuspended in ice-cold lysis buffer (50 mM HEPES pH 7.0, 150 mM NaCl, 5 mM $MgCl_2$, 10 mM imidazole, 1 mg ml^{-1} lysozyme, 1 mM phenylmethylsulfonylfluoride and 5% glycerol) and lysed by sonication. Lysate was centrifuged at 15,000 rpm for 15 min at 4 °C. Soluble material was batch bound for 2 h with 50 μl of Ni-NTA HisBind Resin. The resin was then washed three times with 1 ml wash buffer (50 mM HEPES pH 7.0, 150 mM NaCl, 5 mM $MgCl_2$, 10 mM imidazole and 5% glycerol) and eluted with wash buffer supplemented with 250 mM imidazole. RNA was purified using the Direct-zol RNA miniprep kit (Zymo Research). Samples were resolved by denaturing 15% TBE-Urea PAGE, stained with SYBR Gold according to the manufacturer's instructions, and imaged on an Azure Biosystems Azure 600 imager.

Northern blots

RNA was isolated from 3 ml *L. seeligeri* culture and grown to optical density at 600 nm (OD_{600}) = 0.5 using the Direct-zol RNA miniprep kit (Zymo Research). RNA was mixed with an equal volume of 2× RNA loading dye (95% formamide, 18.8 mM EDTA and 0.02% bromophenol blue), heated to 95 °C for 5 min and then cooled on ice for 1 min. Then, 10 μg total RNA from each sample was resolved by denaturing 15% TBE-Urea PAGE and was transferred overnight to BrightStar nylon membranes (Invitrogen). Membranes were UV-crosslinked, then pre-hybridized in

Ultrahyb buffer (Invitrogen) for 30 min at 42 °C, followed by the addition of 250 pmol Cy3-labelled ssDNA probe and incubate overnight at 42 °C. Hybridized membranes were washed, and then scanned on an Azure Sapphire imager.

Phage propagation

All phage infections were performed in BHI medium supplemented with 5 mM $CaCl_2$. To generate phage lysates, existing phage stocks were diluted to single plaques on a lawn of *L. seeligeri* LS1 *ΔRM1 ΔRM2* and a single plaque was purified twice to ensure homogeneity. Then, 5 ml of cell culture was infected with phage at a multiplicity of infection of 0.1 and OD 0.1, and the infection proceeded overnight. The lysate was centrifuged for 20 min at 4,000 rpm and the supernatant was filtered using a 0.45-µm-pore syringe filter.

Bioinformatic identification of viral cas genes

The IMGVR7.1 database of high-confidence viral genomes[27] was probed for sequences with homology to 536 Cas protein query sequences, representing all known CRISPR subtypes[36]. Each query was searched against IMGVR7.1 using tblastn[33] with an E-value cutoff of 1×10^{-4}. We retrieved 20 kb of genomic sequence flanking each hit gene using bedtools[37], and hits were deduplicated using genometools sequniq[38]. Hit genomic regions were analysed for bona fide CRISPR–Cas systems using CRISPRCasTyper[39], and all hits containing either predicted CRISPR arrays or cas gene operons were removed from analysis. Hits were further filtered to remove any cas genes located within 1 kb of a contig end, and hits sharing greater than 90% nucleotide sequence identity were collapsed using T-Coffee seq_reformat[34]. Finally, the IMGVR7.1 database was probed as above for homologues of known Acrs, anti-restriction-modification[40], anti-Hachiman[41], anti-Gabija and anti-Thoeris genes, and hits within 10 kb of a predicted cas gene were tabulated. The UViG identifier for each hit was used to retrieve predicted host phylogeny from IMGVR. For gene loci diagrams, open reading frames were predicted with prokka[42] and diagrams were generated with Clinker[43].

Statistics and reproducibility

Plasmid-targeting assays shown in Figs. 1b, 2b, 3b, 4c and 5d and Extended Data Figs. 1, 2, 3, 4, 10, 11b,c,j and 12a are each representative images of three biological replicates. Co-immunoprecipitation blots shown in Fig. 3e–g and Extended Data Fig. 12b are each representative images of three biological replicates. RNA gels shown in Figs. 4f,g and 5f and Extended Data Fig. 12c–e are each representative images of three biological replicates.

Reporting summary

Further information on research design is available in the Nature Portfolio Reporting Summary linked to this article.

Data availability

All data supporting the findings of this study are available within the paper and its Supplementary Information. Uncropped gel images corresponding to the experiments reported in this study are available in Supplementary Fig. 1.

33. Altschul, S. F., Gish, W., Miller, W., Myers, E. W. & Lipman, D. J. Basic local alignment search tool. *J. Mol. Biol.* **215**, 403–410 (1990).
34. Notredame, C., Higgins, D. G. & Heringa, J. T-Coffee: a novel method for fast and accurate multiple sequence alignment. *J. Mol. Biol.* **302**, 205–217 (2000).
35. Tamura, K., Stecher, G. & Kumar, S. MEGA11: molecular evolutionary genetics analysis version 11. *Mol. Biol. Evol.* **38**, 3022–3027 (2021).
36. Makarova, K. S. et al. Evolutionary classification of CRISPR–Cas systems: a burst of class 2 and derived variants. *Nat. Rev. Microbiol.* **18**, 67–83 (2020).
37. Quinlan, A. R. & Hall, I. M. BEDTools: a flexible suite of utilities for comparing genomic features. *Bioinformatics* **26**, 841–842 (2010).
38. Lee, W. & Chen, S. L. Genome-tools: a flexible package for genome sequence analysis. *Biotechniques* **33**, 1334–1341 (2002).
39. Russel, J., Pinilla-Redondo, R., Mayo-Munoz, D., Shah, S. A. & Sorensen, S. J. CRISPRCasTyper: automated identification, annotation, and classification of CRISPR–Cas loci. *CRISPR J.* **3**, 462–469 (2020).
40. Krüger, D. H., Schroeder, C., Hansen, S. & Rosenthal, H. A. Active protection by bacteriophages T3 and T7 against E. coli B- and K-specific restriction of their DNA. *Mol. Gen. Genet.* **153**, 99–106 (1977).
41. Yirmiya, E. et al. Phages overcome bacterial immunity via diverse anti-defence proteins. *Nature* **625**, 352–359 (2024).
42. Seemann, T. Prokka: rapid prokaryotic genome annotation. *Bioinformatics* **30**, 2068–2069 (2014).
43. Gilchrist, C. L. M. & Chooi, Y. H. clinker & clustermap.js: automatic generation of gene cluster comparison figures. *Bioinformatics* **37**, 2473–2475 (2021).

Acknowledgements We thank all members of the Meeske lab for advice and encouragement, and members of the Guo and Mitchell labs for helpful discussions. This work in the AJM lab was supported by the NIH (R35GM142460, S10OD026741), NSF (FAIN2235762) and the University of Washington Royalty Research Foundation. A.J.M. is a Rita Allen Foundation Scholar. S.R.M. is supported by the Jane Coffin Childs Memorial Fund for Medical Research. The work in the JBD lab was supported by the National Institutes of Health (R01GM127489) and funding from the Defense Advanced Research Projects Agency (DARPA) award HR0011-17-2-0043. The views, opinions and/or findings expressed are those of the authors and should not be interpreted as representing the official views or policies of the Department of Defense or the US Government, and the DARPA Safe Genes programme (HR0011-17-2-0043).

Author contributions The project was conceived by A.J.M. Acr screen and validation experiments were performed by M.A.K., E.M.S., L.O., A.K., M.C.W., S.R.M. and A.J.M. Experiments to characterize the AcrIB3 and AcrVIA2 mechanism were performed by M.A.K., E.M.S. and A.J.M. Bioinformatic analysis was conducted by M.A.K., M.J., J.B.-D. and A.J.M. M.J. was supervised by J.B.-D. The manuscript was written by M.A.K., E.M.S. and A.J.M. All authors contributed to manuscript editing.

Competing interests A.J.M. is a co-founder of Profluent Bio. J.B.-D. is a scientific advisory board member of SNIPR Biome and Excision Biotherapeutics, a consultant to LeapFrog Bio and a scientific advisory board member and co-founder of Acrigen Biosciences. The Bondy-Denomy lab received research support from Felix Biotechnology. The other authors declare no competing interests.

Additional information

Supplementary information The online version contains supplementary material available at https://doi.org/10.1038/s41586-024-07923-x.

Correspondence and requests for materials should be addressed to Alexander J. Meeske.

Peer review information *Nature* thanks Chase Beisel and the other, anonymous, reviewer(s) for their contribution to the peer review of this work.

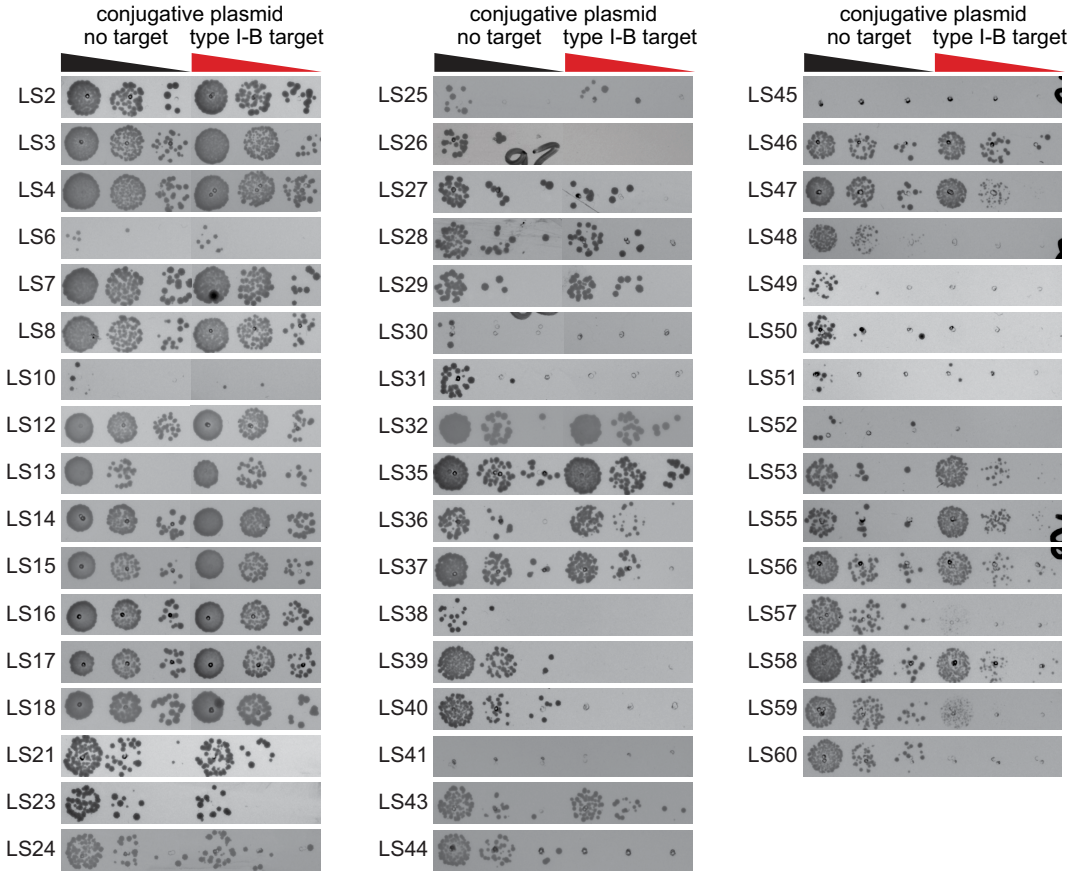

Extended Data Fig. 1 | Variation in *L. seeligeri* strain background affects type I-B CRISPR-Cas immunity. Plasmid targeting assay in which the indicated *L. seeligeri* strains were first transformed with a chromosomally integrated type I-B CRISPR-Cas system equipped with a spacer targeting a conjugative plasmid, then challenged with either a non-target plasmid (left columns) or plasmid containing a target protospacer (right columns).

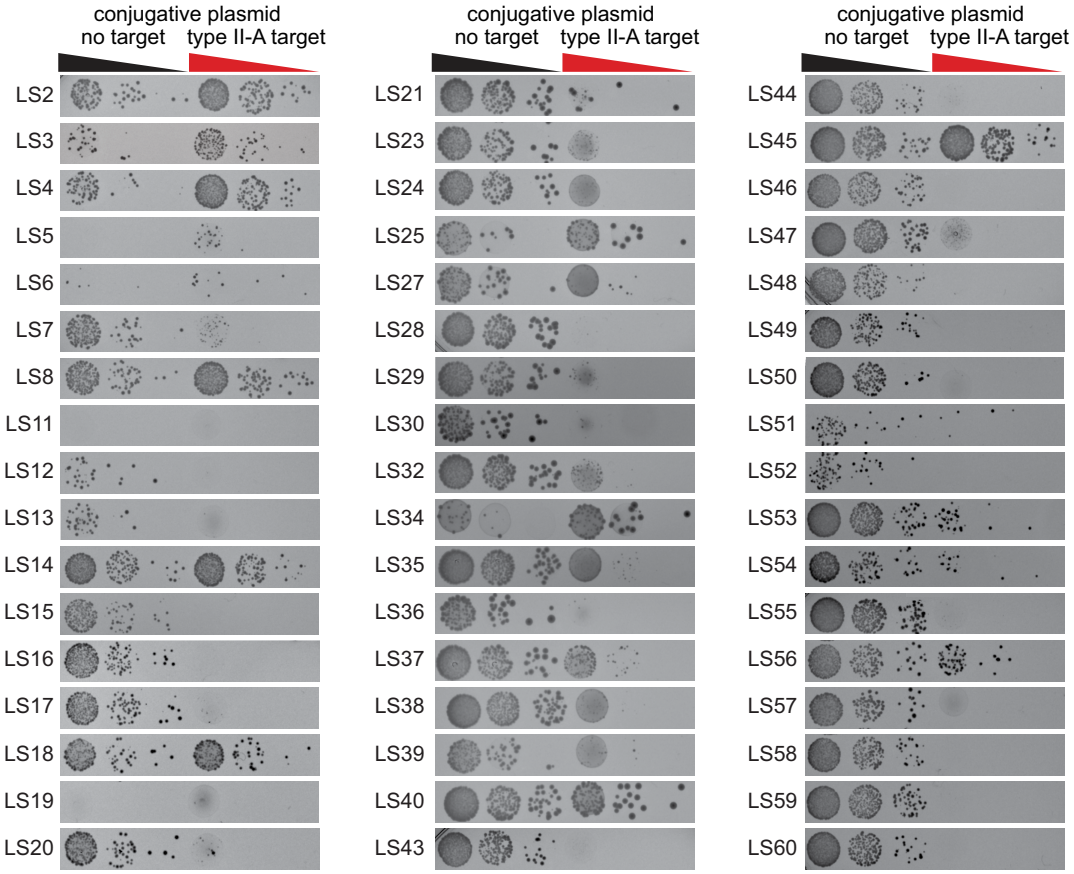

Extended Data Fig. 2 | Variation in *L. seeligeri* strain background affects type II-A CRISPR-Cas immunity. Plasmid targeting assay in which the indicated *L. seeligeri* strains were first transformed with a chromosomally integrated type II-A CRISPR-Cas system equipped with a spacer targeting a conjugative plasmid, then challenged with either a non-target plasmid (left columns) or plasmid containing a target protospacer (right columns).

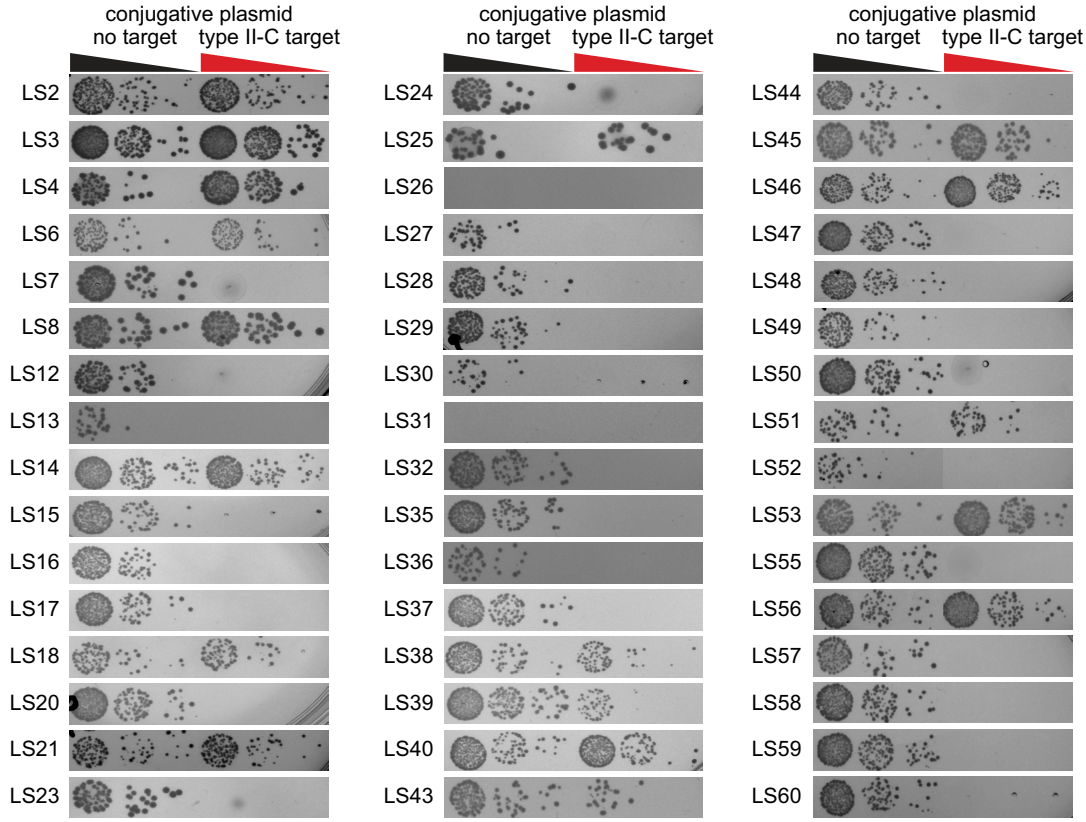

Extended Data Fig. 3 | Variation in *L. seeligeri* strain background affects type II-C CRISPR-Cas immunity. Plasmid targeting assay in which the indicated *L. seeligeri* strains were first transformed with a chromosomally integrated type II-C CRISPR-Cas system equipped with a spacer targeting a conjugative plasmid, then challenged with either a non-target plasmid (left columns) or plasmid containing a target protospacer (right columns).

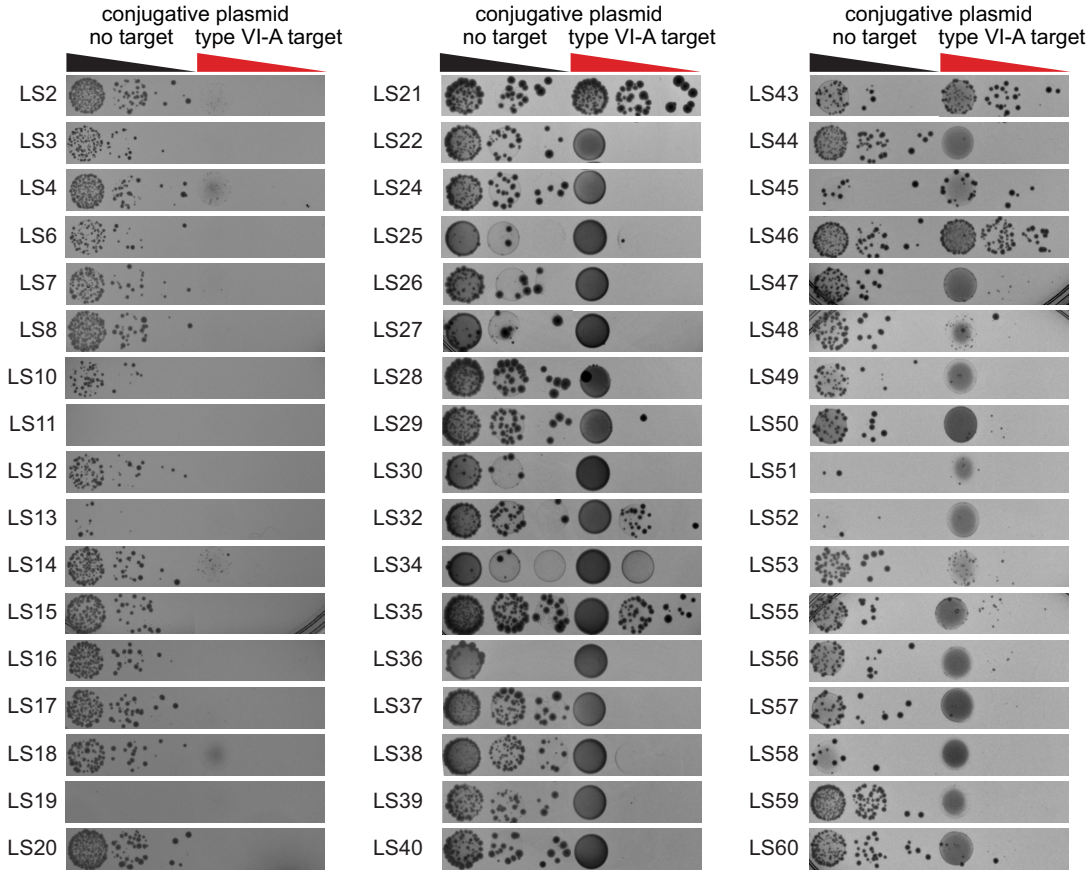

Extended Data Fig. 4 | Variation in *L. seeligeri* strain background affects type VI-A CRISPR-Cas immunity. Plasmid targeting assay in which the indicated *L. seeligeri* strains were first transformed with a chromosomally integrated type VI-A CRISPR-Cas system equipped with a spacer targeting a conjugative plasmid, then challenged with either a non-target plasmid (left columns) or plasmid containing a target protospacer (right columns).

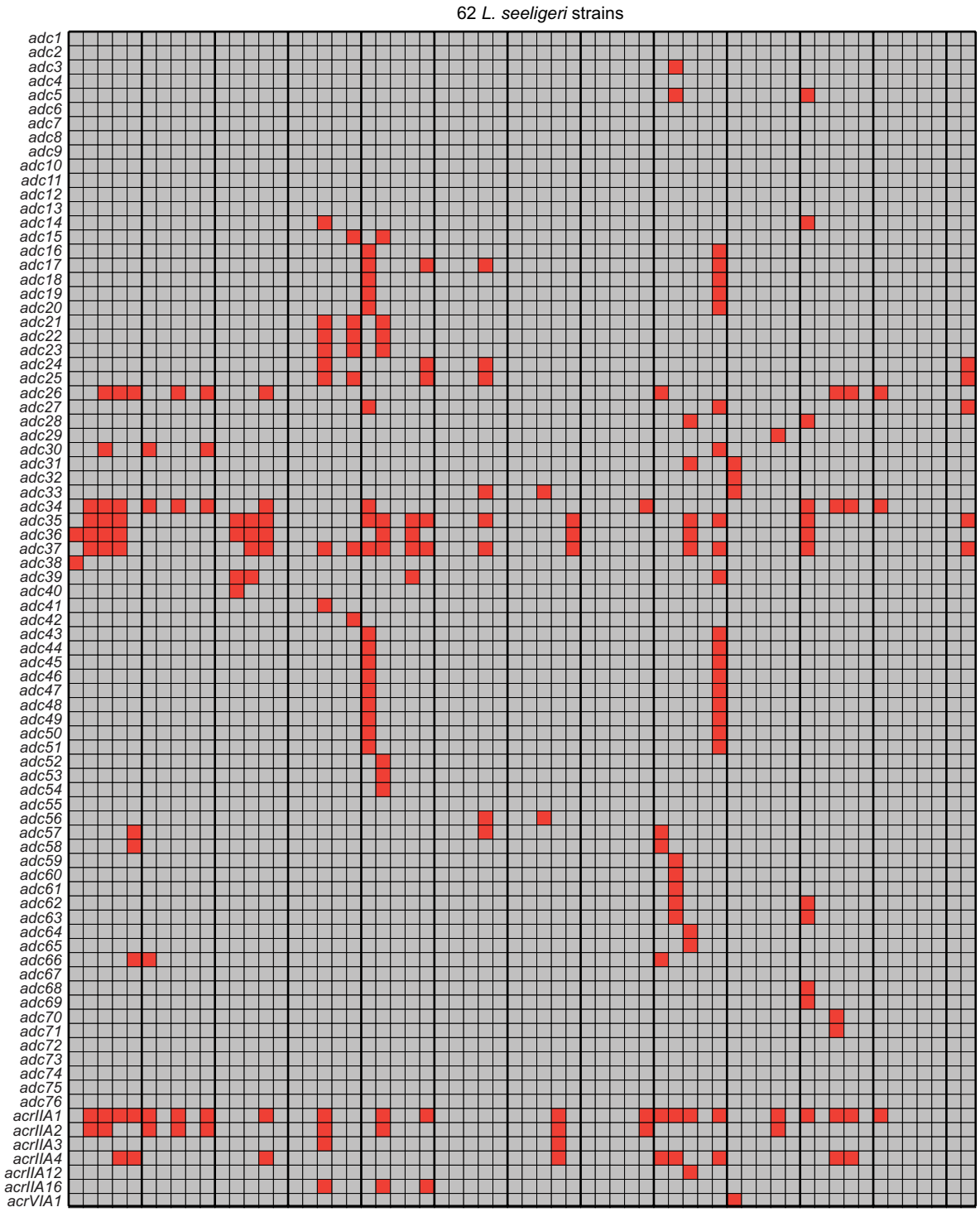

Extended Data Fig. 5 | Anti-defense candidate (adc) gene occurrence across 62 strains of *L. seeligeri*. Each row corresponds to either a known anti-CRISPR gene or a particular anti-defense candidate gene identified as frequently encoded nearby acr genes or nearby other well-established anti-defense candidates. Each column corresponds to an individual *L. seeligeri* strain genome. Filled red boxes indicate occurrence of a putative anti-defense gene in a particular strain.

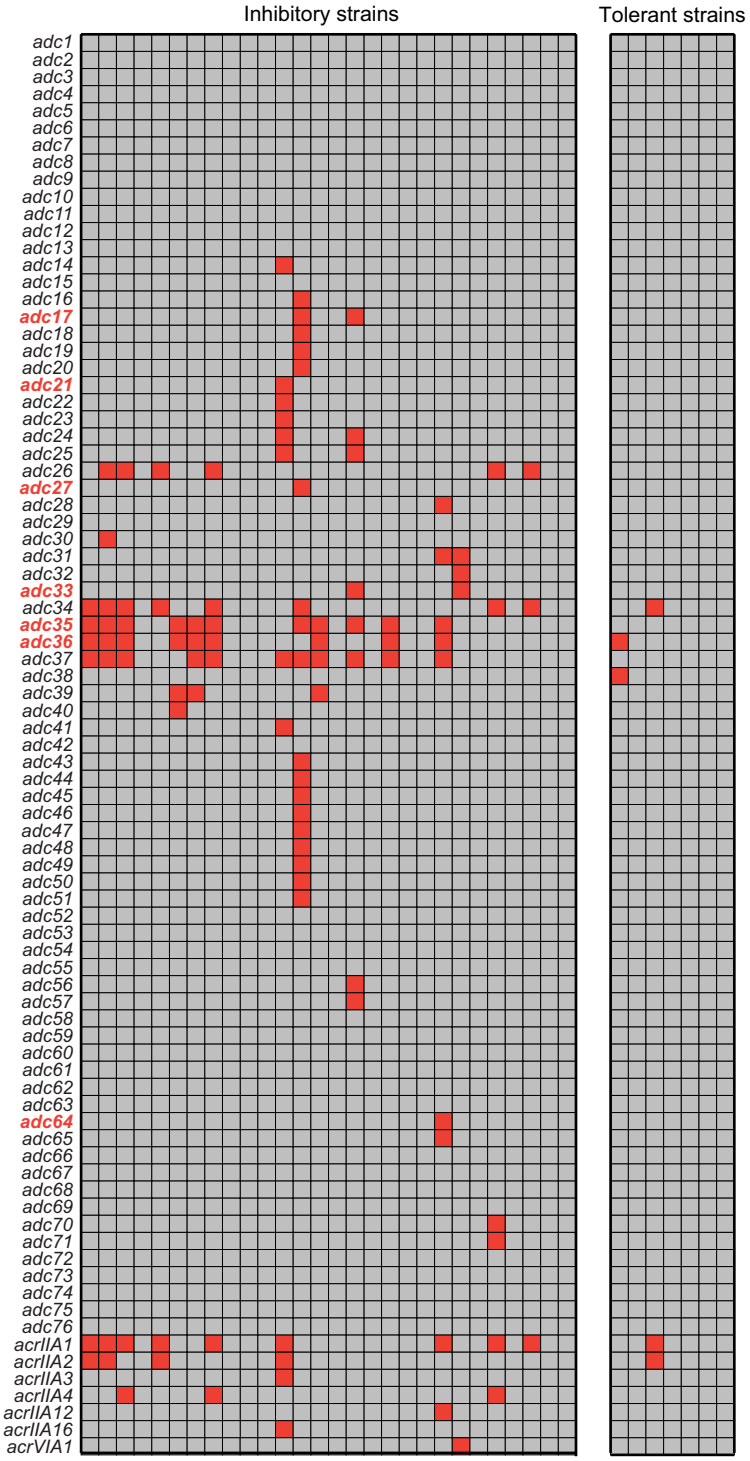

Extended Data Fig. 6 | Anti-defense candidate (adc) gene occurrence among *L. seeligeri* strains that inhibit (or tolerate) type I-B CRISPR immunity. Each row corresponds to either a known anti-CRISPR gene or a particular anti-defense candidate gene identified as frequently encoded nearby acr genes or nearby other well-established anti-defense candidates. Each column corresponds to an individual *L. seeligeri* strain genome. The group of columns on the left indicate strains that inhibited type I-B CRISPR immunity in the plasmid targeting assay shown in Fig. 1, while the group on the right tolerated type I-B immunity. Filled red boxes indicate occurrence of a putative anti-defense gene in a particular strain. Gene names in red indicate experimentally validated type I-B Acrs from this study.

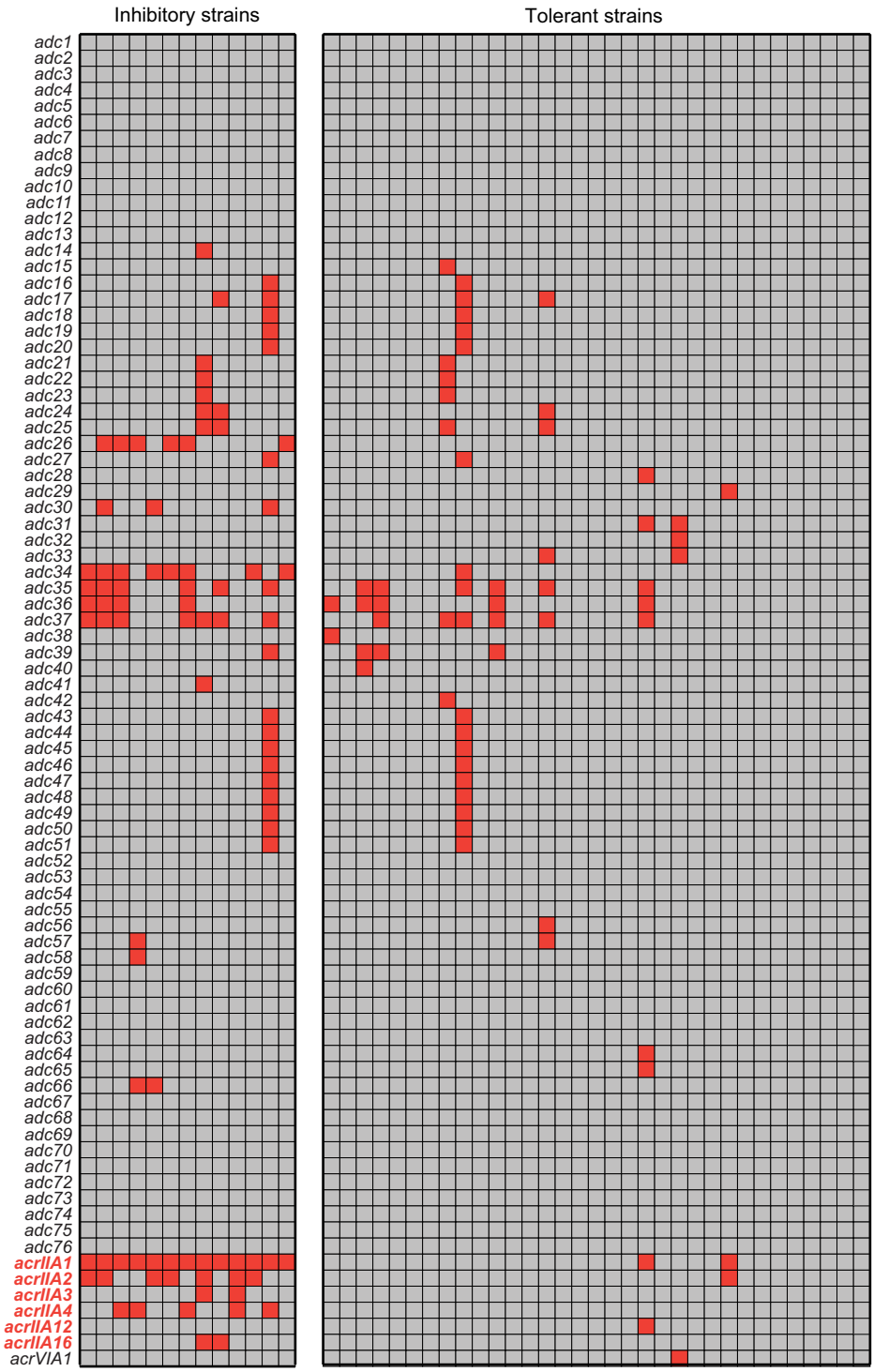

Extended Data Fig. 7 | Anti-defense candidate (adc) gene occurrence among *L. seeligeri* strains that inhibit (or tolerate) type II-A CRISPR immunity. Each row corresponds to either a known anti-CRISPR gene or a particular anti-defense candidate gene identified as frequently encoded nearby acr genes or nearby other well-established anti-defense candidates. Each column corresponds to an individual *L. seeligeri* strain genome. The group of columns on the left indicate strains that inhibited type II-A CRISPR immunity in the plasmid targeting assay shown in Fig. 1, while the group on the right tolerated type II-A immunity. Filled red boxes indicate occurrence of a putative anti-defense gene in a particular strain. Gene names in red indicate experimentally validated type II-A Acrs.

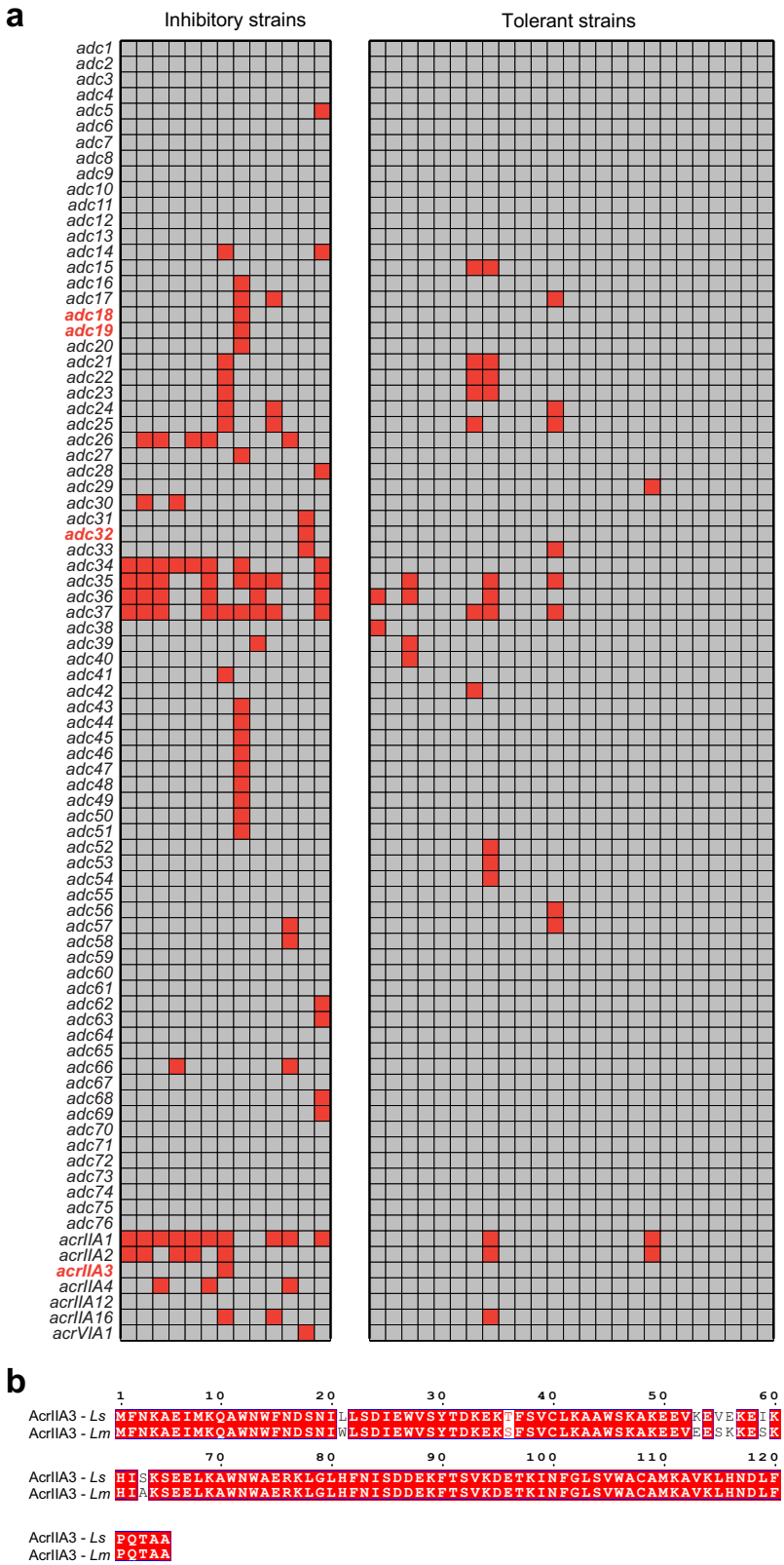

Extended Data Fig. 8 | Anti-defense candidate (adc) gene occurrence among *L. seeligeri* strains that inhibit (or tolerate) type II-C CRISPR immunity. (a) Each row corresponds to either a known anti-CRISPR gene or a particular anti-defense candidate gene identified as frequently encoded nearby acr genes or nearby other well-established anti-defense candidates. Each column corresponds to an individual *L. seeligeri* strain genome. The group of columns on the left indicate strains that inhibited type II-C CRISPR immunity in the plasmid targeting assay shown in Fig. 1, while the group on the right tolerated type II-C immunity. Filled red boxes indicate occurrence of a putative anti-defense gene in a particular strain. Gene names in red indicate experimentally validated type II-C Acrs from this study. (b) Alignment of AcrIIA3 from *L. seeligeri*, which inhibited type II-C but not type II-A CRISPR in our study, with AcrIIA3 from *L. monocytogenes*, which has been shown to inhibit type II-A CRISPR (Rauch et al.[3]).

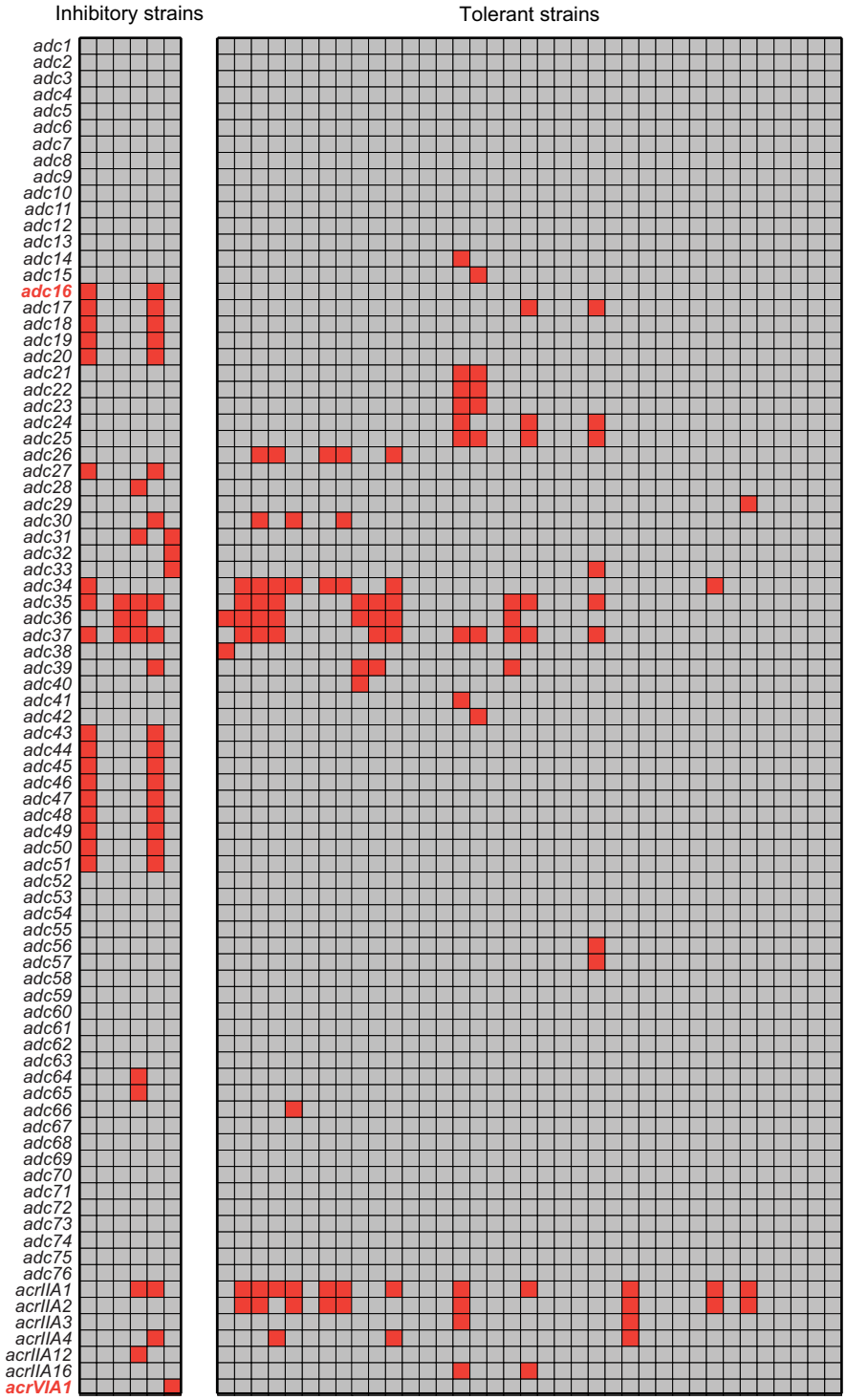

Extended Data Fig. 9 | Anti-defense candidate (adc) gene occurrence among *L. seeligeri* strains that inhibit (or tolerate) type VI-A CRISPR immunity. Each row corresponds to either a known anti-CRISPR gene or a particular anti-defense candidate gene identified as frequently encoded nearby acr genes or nearby other well-established anti-defense candidates. Each column corresponds to an individual *L. seeligeri* strain genome. The group of columns on the left indicate strains that inhibited type VI-A CRISPR immunity in the plasmid targeting assay shown in Fig. 1, while the group on the right tolerated type VI-A immunity. Filled red boxes indicate occurrence of a putative anti-defense gene in a particular strain. Gene names in red indicate experimentally validated type VI-A Acrs from this study.

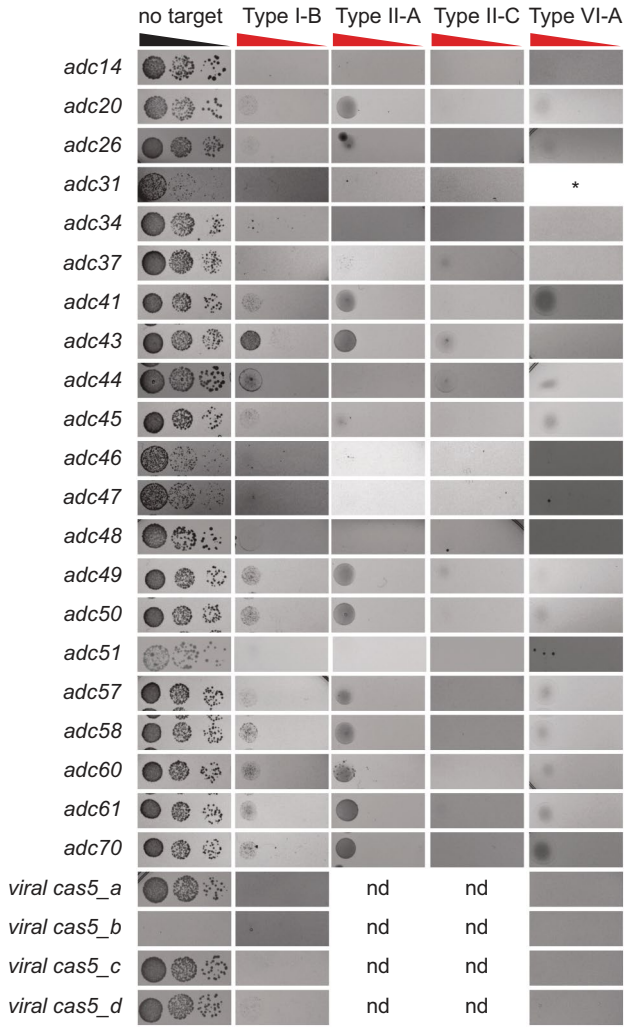

Extended Data Fig. 10 | Anti-Defense Candidates with no detectable anti-CRISPR activity. Each anti-defense candidate was tested for inhibition of plasmid targeting by the indicated CRISPR type in *L. seeligeri* strain LS1. Adcs were first introduced into LS1 carrying the indicated CRISPR type, then a targeted conjugative plasmid was introduced, and the cells were plated on media selecting for the target plasmid. *We previously tested adc31 against the *L. seeligeri* type VI-A CRISPR system in Meeske & Jia et al. Science 2020 (Fig. 1c, pgp1), no inhibition was detected. nd, not determined. Each image is a representative of three biological replicates.

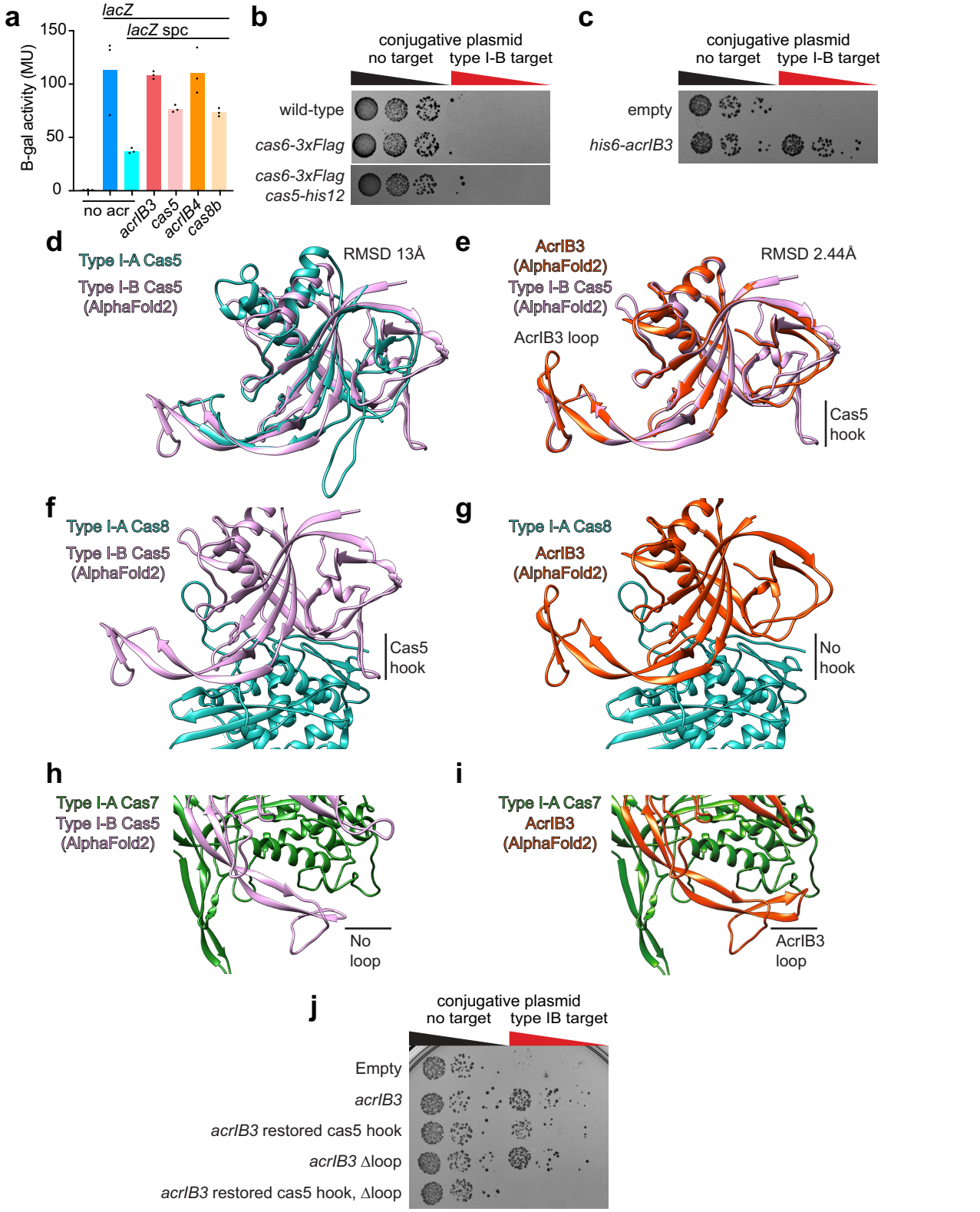

Extended Data Fig. 11 | Predicted structural differences between AcrIB3 and Cas5 are essential for Acr function. (a) Quantitative beta-galactosidase assay corresponding to strains tested in Fig. 3d. (b) Cas6-3xFlag and Cas5-his12 function in immunity against a plasmid containing a protospacer recognized by the type I-B CRISPR system. (c) His6-AcrIB3 functions in inhibition of type I-B CRISPR immunity in the plasmid targeting assay. (d) AlphaFold2 structural model of *L. seeligeri* Cas5 (pink) superimposed onto structure of Cas5 from *Pyrococcus furiosus* type I-A Cascade (cyan). Structure from Hu et al. 2022 Mol. Cell. RMSD, root mean squared deviation. (e) Overlay of *L. seeligeri* Cas5 (pink) and AcrIB3 (orange) structural predictions. Two key structural distinctions are highlighted: a "hook" in Cas5 that is missing from AcrIB3, and an extended loop specific to AcrIB3. (f) *L. seeligeri* Cas5 (pink) modeled into the *P. furiosus* Cascade complex, with Cas8 shown (cyan). Cas5 hook is predicted to contact Cas8. (g) Same as (f), but with AcrIB3 (orange) instead of Cas5. (h) *L. seeligeri* Cas5 (pink) modeled into the *P. furiosus* Cascade complex, with nearest Cas7 protomer shown (green). (i) Same as (h), but with AcrIB3 (orange) instead of Cas5. Extended AcrIB3 loop is predicted to contact Cas7. (j) Plasmid targeting assay demonstrating that restoration of the Cas5 hook in AcrIB3 and deletion of the AcrIB3 loop extension abolishes Acr activity. Representative example of three biological replicates is shown.

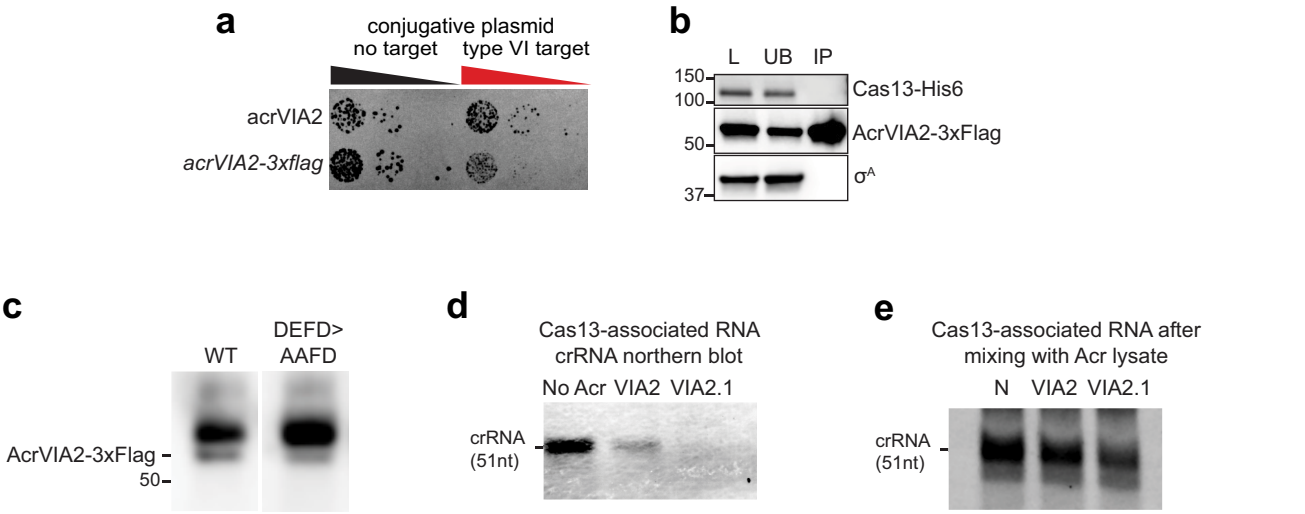

Extended Data Fig. 12 | No detectable interaction between AcrVIA2 and Cas13, and lack of AcrVIA2 activity on pre-formed RNP complexes. (a) AcrVIA2-3xFlag is partially functional in inhibition of immunity against a plasmid expressing an RNA protospacer recognized by the type VI-A CRISPR system. (b) No detectable co-immunoprecipitation of Cas13-his6 and AcrVIA2-3xFlag. The housekeeping sigma factor σA is shown as a non-interacting control. L, load, UB, unbound, IP, immunoprecipitate. Molecular weight in kDa. (c) Anti-Flag immunoblots of 3xFlag tagged WT AcrVIA2 and DEFD > AAFD mutant allele. Molecular weight in kDa. (d) Northern blot analysis of RNA co-immunoprecipitated with Cas13-his6 using crRNA-specific probe. Molecular weight in nucleotides. (e) No effect of AcrVIA2 on crRNAs from pre-formed Cas13:crRNA RNP complexes. Lysates expressing dCas13-his6 were incubated with lysates expressing either no Acr, AcrVIA2, or AcrVIA2.1 for 1 hr at 30 °C in the presence of 1 mM ATP. Cas13 was then immunoprecipitated, and Cas13-associated RNAs were extracted, separated by denaturing PAGE, and analyzed by SYBR Gold staining. Molecular weight in nucleotides.

nature portfolio

Corresponding author(s): Alexander Meeske

Last updated by author(s): Jul 21, 2024

Reporting Summary

Nature Portfolio wishes to improve the reproducibility of the work that we publish. This form provides structure for consistency and transparency in reporting. For further information on Nature Portfolio policies, see our Editorial Policies and the Editorial Policy Checklist.

Statistics

For all statistical analyses, confirm that the following items are present in the figure legend, table legend, main text, or Methods section.

n/a	Confirmed
☐	☒ The exact sample size (*n*) for each experimental group/condition, given as a discrete number and unit of measurement
☐	☒ A statement on whether measurements were taken from distinct samples or whether the same sample was measured repeatedly
☐	☒ The statistical test(s) used AND whether they are one- or two-sided *Only common tests should be described solely by name; describe more complex techniques in the Methods section.*
☒	☐ A description of all covariates tested
☒	☐ A description of any assumptions or corrections, such as tests of normality and adjustment for multiple comparisons
☒	☐ A full description of the statistical parameters including central tendency (e.g. means) or other basic estimates (e.g. regression coefficient) AND variation (e.g. standard deviation) or associated estimates of uncertainty (e.g. confidence intervals)
☒	☐ For null hypothesis testing, the test statistic (e.g. *F*, *t*, *r*) with confidence intervals, effect sizes, degrees of freedom and *P* value noted *Give P values as exact values whenever suitable.*
☒	☐ For Bayesian analysis, information on the choice of priors and Markov chain Monte Carlo settings
☒	☐ For hierarchical and complex designs, identification of the appropriate level for tests and full reporting of outcomes
☒	☐ Estimates of effect sizes (e.g. Cohen's *d*, Pearson's *r*), indicating how they were calculated

Our web collection on statistics for biologists contains articles on many of the points above.

Software and code

Policy information about availability of computer code

Data collection

Bioinformatic identification of viral cas genes:
The IMGVR7.1 database of high-confidence viral genomes was probed for sequences with homology to 536 Cas protein query sequences, representing all known CRISPR subtypes. Each query was searched against IMGVR7.1 using tblastn (BLAST v2.7.1+) with an E-value cutoff of 1x10-4. 20 kb of genomic sequence flanking each hit gene was retrieved using bedtools(v.2.30.0), and hits were deduplicated using genometools sequniq (v.1.6.2). Hit genomic regions were analyzed for bona fide CRISPR-Cas systems using CRISPRCasTyper, and all hits containing either predicted CRISPR arrays or cas gene operons were removed from analysis. Hits were further filtered to remove any cas genes located within 1 kb of a contig end, and hits sharing greater than 90% nucleotide sequence identity were collapsed using T-Coffee seq_reformat (v12.00.7fb08c2). Finally, the IMGVR7.1 database was probed as above for homologs of known Acrs, anti-restriction-modification, anti-Hachiman, anti-Gabija, and anti-Thoeris genes, and hits within 10 kb of a predicted cas gene were tabulated. The UViG identifier for each hit was used to retrieve predicted host phylogeny from IMGVR. For gene loci diagrams, ORFs were predicted with prokka (v1.14.6) and diagrams were generated with Clinker(v0.0.29).

Data analysis

Phylogenetic tree construction:
To reconstruct Acr phylogeny, query Acr proteins were searched against the BLAST nr database using an E-value cutoff of 5x10-3 (for AcrIB4) or 1x10-4 (for all other Acrs). The top 250 hits were aligned using T-Coffee(v12.00.7fb08c2). For AcrIB4, only the C-terminal 90 amino acids were included for alignment, as this is the region with shared homology between AcrIB4 and the much larger Cas8b. Phylogenetic trees and bootstrap values were calculated using MEGA (v11), using the neighbor-joining method with 1000 bootstrap replications.

For manuscripts utilizing custom algorithms or software that are central to the research but not yet described in published literature, software must be made available to editors and reviewers. We strongly encourage code deposition in a community repository (e.g. GitHub). See the Nature Portfolio guidelines for submitting code & software for further information.

Data

Policy information about availability of data

All manuscripts must include a data availability statement. This statement should provide the following information, where applicable:

- Accession codes, unique identifiers, or web links for publicly available datasets
- A description of any restrictions on data availability
- For clinical datasets or third party data, please ensure that the statement adheres to our policy

All data supporting the findings of this study are available within the paper and its Supplementary Information. Uncropped gel images corresponding to the experiments reported in this study are available in Supplementary Fig. 1.

Research involving human participants, their data, or biological material

Policy information about studies with human participants or human data. See also policy information about sex, gender (identity/presentation), and sexual orientation and race, ethnicity and racism.

Reporting on sex and gender	Not relevant to this study.
Reporting on race, ethnicity, or other socially relevant groupings	Not relevant to this study.
Population characteristics	Not relevant to this study.
Recruitment	Not relevant to this study.
Ethics oversight	Not relevant to this study.

Note that full information on the approval of the study protocol must also be provided in the manuscript.

Field-specific reporting

Please select the one below that is the best fit for your research. If you are not sure, read the appropriate sections before making your selection.

☒ Life sciences ☐ Behavioural & social sciences ☐ Ecological, evolutionary & environmental sciences

For a reference copy of the document with all sections, see nature.com/documents/nr-reporting-summary-flat.pdf

Life sciences study design

All studies must disclose on these points even when the disclosure is negative.

Sample size	Sample sizes were not statistically predetermined. All experiments were performed with sample sizes based on standard protocols in the field.
Data exclusions	No data were excluded from the analysis.
Replication	All experimental findings were reliably replicated in biological triplicate.
Randomization	Animal or human research subjects were not involved in this study. None of the experiments were randomized.
Blinding	Animal or human research subjects were not involved in this study. None of the investigators were blinded.

Reporting for specific materials, systems and methods

We require information from authors about some types of materials, experimental systems and methods used in many studies. Here, indicate whether each material, system or method listed is relevant to your study. If you are not sure if a list item applies to your research, read the appropriate section before selecting a response.

Materials & experimental systems

n/a	Involved in the study
☐	☒ Antibodies
☒	☐ Eukaryotic cell lines
☒	☐ Palaeontology and archaeology
☒	☐ Animals and other organisms
☒	☐ Clinical data
☒	☐ Dual use research of concern
☒	☐ Plants

Methods

n/a	Involved in the study
☒	☐ ChIP-seq
☒	☐ Flow cytometry
☒	☐ MRI-based neuroimaging

Antibodies

Antibodies used

IP fractions were analyzed by immunoblot using anti-Flag (Sigma-Aldrich #B3111, used at 1:10,000), anti-His6 (Genscript #A00186, used at 1:4,000), and anti-σA (gift of David Rudner, Harvard Medical School, used at 1:10,000) antibodies.

Validation

Anti-Flag and anti-His6 antibodies were validated on the basis of untagged controls. Anti-σA was used as a loading control, validated through affinity purification with B. subtilis σA protein.